Structural design optimization under dynamic reliability constraints based on probability density evolution method and quantum-inspired optimization algorithm

Li-Li Weng[a], Jia-Shu Yang[a], Jian-Bing Chen[a,*], Michael Beer[b]

[a] *State Key Laboratory of Disaster Reduction in Civil Engineering & College of Civil Engineering, Tongji University, Shanghai 200092, PR China*

[b] *Institute for Risk and Reliability, Leibniz Universität Hannover, Germany & Institute for Risk and Uncertainty, University of Liverpool, United Kingdom*

Abstract:

Dynamic-reliability-based design optimization (DRBDO) has been a promising approach for designing structures under dynamic excitations in the presence of uncertainties. This paper proposes an effective scheme for solving a class of DRBDO problems. The proposed scheme is based on the quantum particle swarm optimization (QPSO) algorithm, a quantum-inspired algorithm that utilizes quantum mechanisms to achieve better exploration and exploitation. During the optimization process, the probability density evolution method (PDEM) combined with the extreme value distribution strategy is employed to evaluate the structural dynamic reliability. Due to the high efficiency of the PDEM, the computational cost associated with reliability assessments can be considerably reduced. Numerical examples involving linear and nonlinear structures with different types of design variables are presented to demonstrate the effectiveness and efficiency of the proposed scheme.

Keywords:

Dynamic-reliability-based design optimization, Dynamic reliability, Probability density evolution method, Quantum particle swarm optimization

* Corresponding author.

E-mail address: chenjb@tongji.edu.cn (J.-B. Chen).

1 Introduction

Structural optimization is widely reckoned a viable design tool for engineering structures (Haftka and Gürdal 1992). However, it has been shown that the performance of a structure is inevitably affected by the uncertainties stemming from material properties and geometrical parameters of the structure, as well as external excitations (Li and Chen 2009). To ensure the optimized structure behaves as expected, the avoidable effects of the uncertainties should be adequately accounted for in the optimization process. In this regard, reliability-based design optimization (RBDO) constitutes an advantageous methodology (Valdebenito and Schuëller 2010), and enormous progress has been made since the 1960s.

Early investigations on RBDO mainly focus on structural design optimization based on the first-order and the second-order reliability methods. Representative works include the reliability index approach (Enevoldsen and Sørensen 1994), the performance measure approach (Tu et al. 1999), the sequential optimization and reliability assessment (SORA) method (Du and Chen 2004), the sequential approximate programming method (Cheng et al. 2006), the single loop approach (Liang et al. 2007), and the hybrid method (Jiang et al. 2017). These methods have proven practical and effective (Aoues and Chateauneuf 2010). However, dynamic excitations, such as earthquakes, sea waves, and wind effects, are usually the dominant causes of structural damage or collapse. This, therefore, necessitates the development of dynamic-reliability-based design optimization (DRBDO) (Jerez et al. 2022).

For DRBDO, a crucial issue is to evaluate the dynamic reliability. Methods for assessing structural dynamic reliability encompass the out-crossing rate-based methods (Coleman 1959), the stochastic simulation methods (Shinozuka 1972; Au and Beck 2001), the moment-based methods (Zhao and Lu 2007), and the probability density-based approaches (Chen and Li 2005), etc. Based on these methods, various DRBDO schemes have been devised. Among them, mathematical programming algorithms and stochastic sampling-based approaches are commonly adopted as optimizers, such as the sequential approximate programming algorithms (Valdebenito and Schuëller 2011), the feasible direction interior point algorithms (Jensen et al. 2013), the stochastic subset optimization algorithms (Taflanidis and Beck 2009), and the transitional Markov chain Monte Carlo (TMCMC)-based approaches (Jensen et al. 2020, 2021). Although DRBDO can be advantageous for achieving reliable structural designs, its application scope is hindered due to the complexity and high computational cost of estimating structural dynamic reliability, especially for nonlinear systems. Moreover, there exist some limitations in the reliability assessment methods mentioned above. For example, the out-crossing rate-based methods rely on certain empirical assumptions

(Lutes and Sarkani 2004), while the moment-based methods may struggle to handle complex structures with small failure probabilities (Lyu and Chen 2021, 2022). Additionally, stochastic simulation methods may not be the most efficient way to estimate the dynamic reliability of high-dimensional systems with strong nonlinear behaviors (Li and Wang 2023). In contrast, the probability density-based approaches exhibit notable benefits. For example, the recently developed Wiener path integral technique can readily determine the stochastic response of high-dimensional nonlinear dynamical systems (Petromichelakis and Kougioumtzoglou 2020), while it demonstrates high accuracy in reliability assessment related to low-probability (failure) events (Psaros and Kougioumtzoglou 2020). Another prominent method is the probability density evolution method (PDEM) (Li and Chen 2004, 2008), which stands as a theoretically rigorous and pragmatic method for structural stochastic response analysis. The PDEM distinguishes itself with its versatility and applicability, especially for general nonlinear systems. Furthermore, the PDEM has already showcased its efficacy in optimization processes (Chen et al. 2020; Yang et al. 2022a, b, c), establishing itself as a powerful tool for design optimization endeavors.

Generally, DRBDO problems can be formulated as constrained optimization problems and solved using mathematical programming algorithms, where the gradient information of objective and constraint functions is required (Yang et al. 2022a). However, the gradients of the implicit reliability constraint functions are analytically intractable for general stochastic nonlinear systems; this is a situation often encountered in engineering practice. One may resort to numerical techniques to approximate the gradients, such as the finite difference method. Nevertheless, selecting a proper step size is cumbersome (Haftka and Adelman 1989). In addition, the reliability constraints may also exacerbate the non-linearity and non-convexity of the optimization problems, which makes the gradient-based algorithms sensitive to initial solutions, prone to get stuck in local optima, or even divergent (fail to converge) (Zhong et al. 2022).

Given this, metaheuristic approaches, e.g., the particle swarm optimization (PSO) algorithm (Kennedy and Eberhart 1995), can tackle challenging optimization problems without the knowledge of gradients and achieve global solutions with a higher probability. Hence, there has been a growing interest in synthesizing metaheuristics into the design optimization of static systems with uncertainties. For example, Dimou and Koumousis (2009) employed binary PSO for the RBDO of statically determinate truss structures; Yang and Hsieh (2011) solved the discrete and non-smooth RBDO problems using an improved PSO algorithm, followed by the standard / multi-objective PSO algorithm that was enhanced by support vector machine (Yang and Hsieh 2013; Yang et al. 2016); Chen et al. (2013) performed the RBDO of composite structures based on PSO and the finite element method; Hamzehkolaei et al. (2016) proposed weighted simulation-assisted PSO to solve the RBDO problems; Liao and Biton (2019) utilized PSO to optimize the structure whose reliability was estimated using an equivalent single variable Pearson's distribution system; Later, they presented a RBDO method combining PSO and a generalized moment-based method for reliability assessments (Liao and Biton 2020). Recent comparative studies on metaheuristics for solving RBDO problems can be found in Meng et al. (2021). As for designing dynamical systems, a few researchers embedded the time-dependent reliability-based methods into metaheuristics and proposed some practical DRBDO frameworks, where the structural reliability was evaluated using the moment-based method (Yu et al. 2019) and the stochastic simulation-based method (Zafar et al. 2020). Nevertheless, research relevant to DRBDO that incorporates metaheuristic algorithms and effective dynamic reliability assessment methods is severely inadequate.

Although metaheuristic algorithms are powerful and versatile, they still have some drawbacks, e.g., premature convergence and low convergence rate. Recently, a new promising family of quantum-inspired metaheuristics that can alleviate these issues has emerged. Different from quantum algorithms that should be executed on quantum computers, these metaheuristics can run on classical computers while taking advantage of quantum mechanisms such as superposition and entanglement. Representative works include the quantum particle swarm optimization (QPSO) algorithm based on the stochastic nature of quantum physics (Sun et al. 2004a), the quantum genetic algorithm based on quantum state superposition (Han and Kim 2000), the quantum annealing algorithm based on quantum tunnelling effect (Kadowaki and Nishimori 1998), etc. Among them, the QPSO algorithm has gained great popularity among researchers spanning diverse disciplines. Its better performance compared to the classical PSO algorithm lies in its fine search ability, reduced requirements for parameter tuning, and decreased likelihood of premature convergence (Sun et al. 2012). Until now, the QPSO algorithm and its improvements have been widely applied to problems on deterministic engineering design (Coelho 2010; Agrawal et al. 2021; Chen et al. 2022), image segmentation (Li et al. 2015), text document clustering (Song et al. 2015), environmental/economic dispatch (Yao et al. 2012; Liu et al. 2016; Zhao et al. 2020), cancer classification (Xi et al. 2016), trajectory planning (Xue et al. 2017), and structural damage recognition (Zhang et al. 2020). The features of the QPSO are beneficial for tackling the challenges associated with DRBDO problems, which are time-consuming to solve and often involve the presence of numerous local optima.

In the present paper, a new DRBDO scheme is proposed. The scheme incorporates the QPSO for solving the optimization problem and the PDEM for evaluating structural dynamic reliability required in the optimization iterations. The design variables can be either deterministic design parameters or distribution parameters of random variables. This study aims to investigate the effectiveness of the proposed scheme for designing linear and nonlinear stochastic structures under dynamic reliability constraints, as well as to assess the computational efficiency and feasibility of the proposed scheme under high-dimensional design variables and multiple constraint conditions. The rest of this paper is organized as follows: Section 2 describes the general formulation of the DRBDO problem to be solved. Section 3 briefly introduces the fundamentals and solution procedures for assessing structural dynamic reliability based on the PDEM. The QPSO algorithm and the proposed DRBDO scheme are presented in Section 4. In Section 5, several numerical examples are presented. The paper closes with some concluding remarks.

2 Formulation of the DRBDO problem

The optimization problems pertinent to this study can be formulated in the following form:

$$\begin{array}{lll} \min\limits_{\boldsymbol{x}} & f(\boldsymbol{x}) & \\ \text{s.t.} & h_j(\boldsymbol{x}) \leqslant 0 & j=1,\cdots,n_{\mathrm{h}} \\ & g_k(\boldsymbol{x}) \leqslant 0 & k=1,\cdots,n_{\mathrm{g}} \\ & \underline{x}_i \leqslant x_i \leqslant \overline{x}_i & i=1,\cdots,n_x \end{array}, \tag{1}$$

where $\boldsymbol{x}=(x_1,x_2,\cdots,x_{n_x})^{\mathrm{T}}$ is the n_x-dimensional vector of design variables with the i-th component x_i belonging to the interval $[\underline{x}_i,\overline{x}_i]$; $f(\boldsymbol{x})$ is the objective function; $h_j(\boldsymbol{x})\leqslant 0$, $j=1,\cdots,n_{\mathrm{h}}$ are the reliability constraints; $g_k(\boldsymbol{x})\leqslant 0$, $k=1,\cdots,n_{\mathrm{g}}$ are the standard constraints; n_x, n_{h} and n_{g} are the numbers of the design variables, the reliability constraints, and the standard constraints, respectively.

For the DRBDO problems, the objective function and the standard constraints are generally related to design requirements (e.g., structural weight, geometric conditions, and construction cost). They are assumed to be explicit and differentiable in terms of the design vector $\boldsymbol{x}$. The reliability constraints are defined in terms of reliability measures. A typical reliability measure for engineering structures subjected to dynamic actions is the first-passage probability. With this reliability measure, the reliability constraint functions in Equation (1) can be rewritten as

$$h_j(\boldsymbol{x}) = P_{F_j}(\boldsymbol{x}) - P_{F_j}^{\mathrm{th}} \leqslant 0, \ (j=1,\cdots,n_{\mathrm{h}}), \tag{2}$$

where $P_{F_j}(\boldsymbol{x})$ denotes the first-passage probability evaluated at the design $\boldsymbol{x}$ for the j-th failure mode F_j, and $P_{F_j}^{\mathrm{th}}$ is the corresponding threshold of the failure probability. The first-passage probability $P_{F_j}(\boldsymbol{x})$ of a structure during the time interval $(0,T]$ is given by

$$P_{F_j}(\boldsymbol{x}) = \Pr\left\{H_j(\boldsymbol{\varTheta},t;\boldsymbol{x}) \in \Omega_{F_j}, \exists t \in (0,T]\right\}, \tag{3}$$

where $H_j(\boldsymbol{\varTheta},t;\boldsymbol{x})$ is the structural response of interest evaluated at the design $\boldsymbol{x}$; $\boldsymbol{\varTheta}=(\varTheta_1,\varTheta_2,\cdots,\varTheta_{n_\varTheta})^{\mathrm{T}}$ denotes the $n_\varTheta$-dimensional random vector; Ω_{F_j} is the failure domain of the failure event F_j; and $\Pr\{\cdot\}$ is the probability operator. In particular, when a symmetrically double-sided boundary is considered, the first-passage probability can be written as

$$P_{F_j}(\boldsymbol{x}) = \Pr\left\{ |H_j(\boldsymbol{\Theta}, t; \boldsymbol{x})| > H_j^{\text{th}}, \exists\, t \in (0, T] \right\}, \tag{4}$$

where $H_j^{\text{th}} > 0$ is the acceptable response threshold. It is noted that the design variables $\boldsymbol{x}$ can be either deterministic design parameters or probability distribution parameters, such as the mean values of the random variables $\boldsymbol{\Theta}$.

3 Reliability analysis with the PDEM

To solve the DRBDO problem outlined in Section 2, the first-passage probability of the structure needs to be estimated. However, this is arduous because extensive structural analyses and a demanding high-dimensional integration are required. In this regard, the PDEM is employed due to its high efficiency and generality. For clarity, the fundamentals of the PDEM-based dynamic reliability assessment are elaborated in this section.

3.1 Fundamentals of the PDEM

Without loss of generality, the equation of motion of an n_d -degree-of-freedom stochastic dynamical system subjected to stochastic excitations reads

$$\boldsymbol{M}(\boldsymbol{\Theta}; \boldsymbol{x})\ddot{\boldsymbol{Y}}(t) + \boldsymbol{C}(\boldsymbol{\Theta}; \boldsymbol{x})\dot{\boldsymbol{Y}}(t) + \boldsymbol{F}(\boldsymbol{\Theta}, \boldsymbol{Y}; \boldsymbol{x}) = \boldsymbol{\Gamma}\boldsymbol{\xi}(\boldsymbol{\Theta}; t), \tag{5}$$

where $\boldsymbol{Y}$, $\dot{\boldsymbol{Y}}$, and $\ddot{\boldsymbol{Y}}$ are the n_d -dimensional displacement, velocity and acceleration vectors, respectively; $\boldsymbol{M}$ and $\boldsymbol{C}$ are the $n_d \times n_d$ mass and damping matrices, respectively; $\boldsymbol{F}$ denotes the n_d -dimensional linear or nonlinear restoring force vector; $\boldsymbol{\Gamma}$ represents the $n_d \times r$ loading influence matrix; $\boldsymbol{\xi}$ is the $r \times 1$ vector of stochastic excitations; $\boldsymbol{x} = (x_1, x_2, \cdots, x_{n_x})^{\mathrm{T}}$ is the design vector; and $\boldsymbol{\Theta} = (\Theta_1, \Theta_2, \cdots, \Theta_{n_\Theta})^{\mathrm{T}}$ is the random vector containing the stochastic parameters involved in structural properties and external excitations. The random vector $\boldsymbol{\Theta}$ is described by a known joint probability density function (PDF) $p_{\boldsymbol{\Theta}}(\boldsymbol{\theta}; \boldsymbol{x})$, and $\boldsymbol{\theta}$ denotes a realization of $\boldsymbol{\Theta}$.

For a well-posed dynamics problem, the solution to Equation (5) exists uniquely and is a function of the design vector $\boldsymbol{x}$ and the random vector $\boldsymbol{\Theta}$. With the solution, a set of physical quantities of interest, such as stresses and displacements, can be obtained. For simplicity, denote them by $\boldsymbol{Z} = (Z_1, Z_2, \cdots, Z_{n_z})^{\mathrm{T}}$. Note that the augmented system $(\boldsymbol{Z}, \boldsymbol{\Theta})$ is probability-preserved, since all randomness has been embedded in the random vector $\boldsymbol{\Theta}$. According to the principle of preservation of probability (Li and Chen 2008; Chen and Li 2009), the joint PDF of $(\boldsymbol{Z}, \boldsymbol{\Theta})$ satisfies the following generalized density evolution equation (GDEE):

$$\frac{\partial p_{\boldsymbol{Z\Theta}}(\boldsymbol{z}, \boldsymbol{\theta}, t; \boldsymbol{x})}{\partial t} + \sum_{i=1}^{n_z} \dot{Z}_i(\boldsymbol{\theta}, t; \boldsymbol{x}) \frac{\partial p_{\boldsymbol{Z\Theta}}(\boldsymbol{z}, \boldsymbol{\theta}, t; \boldsymbol{x})}{\partial z_i} = 0, \tag{6}$$

where $p_{\boldsymbol{Z\Theta}}(\boldsymbol{z},\boldsymbol{\theta},t;\boldsymbol{x})$ is the instantaneous joint PDF of $\boldsymbol{Z}$ and $\boldsymbol{\Theta}$ at time t and the design $\boldsymbol{x}$, and $\dot{Z}_i(\boldsymbol{\theta},t;\boldsymbol{x})$ is the velocity response of Z_i in the case $\boldsymbol{\Theta}=\boldsymbol{\theta}$. The initial condition of Equation (6) is given by

$$p_{\boldsymbol{Z\Theta}}(\boldsymbol{z},\boldsymbol{\theta},t;\boldsymbol{x})|_{t=0}=\delta(\boldsymbol{z}-\boldsymbol{z}_0)p_{\boldsymbol{\Theta}}(\boldsymbol{\theta};\boldsymbol{x}), \tag{7}$$

where $\boldsymbol{z}_0$ denotes the deterministic initial value of $\boldsymbol{Z}$, and $\delta(\cdot)$ is Dirac's delta function.

If only one stochastic response Z of the dynamical system is of interest, the GDEE is reduced to

$$\frac{\partial p_{Z\boldsymbol{\Theta}}(z,\boldsymbol{\theta},t;\boldsymbol{x})}{\partial t}+\dot{Z}(\boldsymbol{\theta},t;\boldsymbol{x})\frac{\partial p_{Z\boldsymbol{\Theta}}(z,\boldsymbol{\theta},t;\boldsymbol{x})}{\partial z}=0 \tag{8}$$

with the initial condition

$$p_{Z\boldsymbol{\Theta}}(z,\boldsymbol{\theta},t;\boldsymbol{x})|_{t=0}=\delta(z-z_0)p_{\boldsymbol{\Theta}}(\boldsymbol{\theta};\boldsymbol{x}), \tag{9}$$

where z_0 is the deterministic initial value of Z. By solving the initial-value problem (Equation (8)) to obtain the joint PDF $p_{Z\boldsymbol{\Theta}}(z,\boldsymbol{\theta},t;\boldsymbol{x})$ and then integrating the PDF over the probability space $\Omega_{\boldsymbol{\Theta}}$, one can obtain the instantaneous PDF of the structural response Z, namely

$$p_Z(z,t;\boldsymbol{x})=\int_{\Omega_{\boldsymbol{\Theta}}}p_{Z\boldsymbol{\Theta}}(z,\boldsymbol{\theta},t;\boldsymbol{x})\mathrm{d}\boldsymbol{\theta}. \tag{10}$$

Since the GDEE (Equation (8)) is only analytically tractable for a few simple cases (Jiang and Li 2016), its approximate solutions are desirable to be obtained by numerical methods for most dynamical systems, for which the closed-form solutions of the velocity response $\dot{Z}$ are not available. Mostly, the finite difference method (FDM) (Chen et al. 2020) is adopted for solving the GDEE, while other methods are also acceptable. For the sake of conciseness, readers are referred to the Appendix for further information about the solution procedures of the GDEE.

3.2 Failure probability assessment of structures

On the basis of the PDEM, the first-passage probability of a structure can be estimated by either the absorbing boundary condition approach (Li and Chen 2005) or the extreme value distribution approach (Chen and Li 2007). Practically, the absorbing boundary condition approach is more applicable to time-dependent reliability problems, whereas the extreme value distribution approach is preferable to systems with multi-failure modes. In light of this, the extreme value distribution approach is employed herein. According to the extreme value distribution approach, for a system with multiple failure modes, the first-passage probability can be evaluated by integrating the PDF of the equivalent extreme-value associated with failure events of the structure (Chen and Li 2007; Li et al. 2007a). Based on the PDEM, this PDF can be conveniently obtained by constructing a virtual stochastic process related to the equivalent extreme-value and then solving the GDEE corresponding to the virtual stochastic process.

For a dynamical system involving $\boldsymbol{\Theta}$ as the basic random vector at the design $\boldsymbol{x}$, suppose that the first-passage probability is defined in terms of structural responses, which are a series of stochastic processes denoted as $\boldsymbol{Z}(\boldsymbol{\Theta},t;\boldsymbol{x})=(Z_1,Z_2,\cdots,Z_{n_z})^{\mathrm{T}}$. Specifically, the structure is assumed to be failed if any component $Z_i(\boldsymbol{\Theta},t;\boldsymbol{x}), i=1,\cdots,n_z$ of $\boldsymbol{Z}(\boldsymbol{\Theta},t;\boldsymbol{x})$ exceeds the corresponding threshold $Z_i^{\mathrm{th}}, i=1,\cdots,n_z$ during the time interval $(0,T_i]$. Thus, as defined by Equation (4), the first-passage probability reads (e.g., a double boundary condition)

$$P_F=\Pr\left\{|Z_i(\boldsymbol{\Theta},t;\boldsymbol{x})|>Z_i^{\mathrm{th}},\exists t\in(0,T_i],\exists i=1,\cdots,n_z\right\}. \tag{11}$$

Denote the time-dependent limit state functions as

$$G_i(\boldsymbol{\Theta},t;\boldsymbol{x})=|Z_i(\boldsymbol{\Theta},t;\boldsymbol{x})|-Z_i^{\mathrm{th}}, i=1,\cdots n_z. \tag{12}$$

Then, Equation (11) can be equivalently written as

$$P_F=\Pr\left\{\bigcap_{i}^{n_z}\bigcap_{t\in(0,T_i]}G_i(\boldsymbol{\Theta},t;\boldsymbol{x})>0\right\}. \tag{13}$$

Define the equivalent extreme value as

$$G_{\mathrm{ext}}(\boldsymbol{\Theta};\boldsymbol{x})=\min_{1\leqslant i\leqslant n_z}\left(\min_{t\in(0,T_i]}G_i(\boldsymbol{\Theta},t;\boldsymbol{x})\right), \tag{14}$$

then the failure probability in Equation (13) can be consequently computed by

$$P_F=\Pr\left\{G_{\mathrm{ext}}(\boldsymbol{\Theta};\boldsymbol{x})>0\right\}. \tag{15}$$

To obtain the PDF of the equivalent extreme value $G_{\mathrm{ext}}(\boldsymbol{\Theta};\boldsymbol{x})$ (Equation (14)) based on the PDEM, a virtual stochastic process associated with $G_{\mathrm{ext}}(\boldsymbol{\Theta};\boldsymbol{x})$ should be first constructed as

$$W(\boldsymbol{\Theta},\tau;\boldsymbol{x})=G_{\mathrm{ext}}(\boldsymbol{\Theta};\boldsymbol{x})\cdot\sin(\omega_{\mathrm{v}}\tau), \tag{16}$$

which satisfies the conditions

$$W(\boldsymbol{\Theta},\tau;\boldsymbol{x})|_{\tau=0}=0, \tag{17}$$

$$W(\boldsymbol{\Theta},\tau;\boldsymbol{x})|_{\tau=\tau_{\mathrm{c}}}=G_{\mathrm{ext}}(\boldsymbol{\Theta};\boldsymbol{x})\cdot\sin(\omega_{\mathrm{v}}\tau_c)=G_{\mathrm{ext}}(\boldsymbol{\Theta};\boldsymbol{x}), \tag{18}$$

where τ is the “virtual time”, $\omega_{\mathrm{v}}=2.5\pi$, and $\tau_{\mathrm{c}}=1$.

Then, deduce the GDEE in terms of the joint PDF of $(\boldsymbol{\Theta},W(\boldsymbol{\Theta},\tau;\boldsymbol{x}))$ as demonstrated in Section 3.1, that is

$$\frac{\partial p_{W\boldsymbol{\Theta}}(w,\boldsymbol{\theta},\tau;\boldsymbol{x})}{\partial\tau}+\dot{W}(\boldsymbol{\theta},\tau;\boldsymbol{x})\frac{\partial p_{W\boldsymbol{\Theta}}(w,\boldsymbol{\theta},\tau;\boldsymbol{x})}{\partial w}=0 \tag{19}$$

with the initial condition

$$p_{W\boldsymbol{\Theta}}(w,\boldsymbol{\theta},\tau;\boldsymbol{x})|_{t=0}=\delta(w)p_{\boldsymbol{\Theta}}(\boldsymbol{\theta};\boldsymbol{x}), \tag{20}$$

where $p_{W\boldsymbol{\Theta}}(w,\boldsymbol{\theta},\tau;\boldsymbol{x})$ is the joint PDF of $(\boldsymbol{\Theta},W(\boldsymbol{\Theta},\tau;\boldsymbol{x}))$, and $\dot{W}$ is the derivative with respect to τ.

Subsequently, the initial-value problem (Equation (19) and (20)) is solved with the numerical procedures presented in the Appendix to obtain the joint PDF $p_{W\boldsymbol{\Theta}}(w,\boldsymbol{\theta},\tau;\boldsymbol{x})$, whose marginal distribution $p_W(w,\tau;\boldsymbol{x})$ is exactly the PDF of the virtual stochastic process $W(\boldsymbol{\Theta},\tau;\boldsymbol{x})$, namely

$$p_W(w,\tau;\boldsymbol{x})=\int_{\Omega_{\boldsymbol{\Theta}}}p_{W\boldsymbol{\Theta}}(w,\boldsymbol{\theta},\tau;\boldsymbol{x})\mathrm{d}\boldsymbol{\theta}. \tag{21}$$

According to Equation (18), one can directly get the PDF of the equivalent extreme value $G_{\mathrm{ext}}(\boldsymbol{\Theta};\boldsymbol{x})$ as

$$p_{G_{\mathrm{ext}}}(g;\boldsymbol{x}) = p_W(w,\tau;\boldsymbol{x})|_{w=g,\tau=\tau_c} . \tag{22}$$

Finally, the first-passage probability (Equation (15)) can be easily evaluated through a one-dimensional integration, i.e.,

$$P_F(\boldsymbol{x}) = \int_0^{+\infty} p_{G_{\mathrm{ext}}}(g;\boldsymbol{x})\mathrm{d}g . \tag{23}$$

4 Optimization strategy

The QPSO algorithm is employed to solve the DRBDO problem in this study. In this section, the principles of both the QPSO and its classical version, PSO, are elaborated. Then the DRBDO scheme integrating the PDEM and the QPSO is proposed.

4.1 The PSO algorithm

The PSO algorithm is a population-based optimization algorithm and has been studied extensively (Freitas et al. 2020). The canonical PSO starts by randomly selecting a population of N_{p} particles, with the position of each particle representing a candidate solution. In the n_x-dimensional search space, the position and the velocity of each particle in the particle swarm are updated based on the best individual positions of particles and the optimal position of the swarm during the optimization process. Denote $\boldsymbol{x}^{(i,\ell)} = (x_1^{(i,\ell)}, x_2^{(i,\ell)}, \cdots, x_{n_x}^{(i,\ell)})^{\mathrm{T}}$ and $\boldsymbol{v}^{(i,\ell)} = (v_1^{(i,\ell)}, v_2^{(i,\ell)}, \cdots, v_{n_x}^{(i,\ell)})^{\mathrm{T}}$ as the position and the velocity of the i-th particle at the ℓ-th iteration, respectively. Then, the position and the velocity can be updated using the standard formulae given by (Shi and Eberhart 1998)

$$\begin{cases} \boldsymbol{v}^{(i,\ell+1)} = \omega_\ell \times \boldsymbol{v}^{(i,\ell)} + c_1 \times r_{1,\ell} \times \left(\mathrm{pbest}^{(i,\ell)} - \boldsymbol{x}^{(i,\ell)}\right) \\ \qquad\qquad + c_2 \times r_{2,\ell} \times \left(\mathrm{gbest}^{(\ell)} - \boldsymbol{x}^{(i,\ell)}\right) \\ \boldsymbol{x}^{(i,\ell+1)} = \boldsymbol{x}^{(i,\ell)} + \boldsymbol{v}^{(i,\ell+1)} \end{cases} , \tag{24}$$

where c_1 and c_2 represent the cognitive learning rate and the social learning rate, respectively; ω_ℓ is the inertia weight decreasing with the generation; $r_{1,\ell}$ and $r_{2,\ell}$ are two independent random numbers uniformly distributed over the interval $[0,1]$; $\mathrm{pbest}^{(i,\ell)}$ is the individual optimal position of the i-th particle; $\mathrm{gbest}^{(\ell)}$ denotes the global best position of the particle swarm; and ℓ is the number of generation. Note that the parameters c_1, c_2 and ω_ℓ should be carefully selected to ensure the stability and the convergence of the PSO.

4.2 The QPSO algorithm

The PSO determines the movement of a particle by its position and velocity (Equation (24)). In the view of classical mechanics, the movement follows a deterministic trajectory if the effects of the random numbers in the algorithm are ignored. Unlike the PSO, the QPSO (Sun et al. 2004a) describes the position of a particle with a wave function, which is inspired by quantum mechanics theories. In quantum mechanics, the state of a physical particle can be fully depicted in a probabilistic way by its wave function. Assuming $\psi(x,t)$ is the wave function of a particle in a one-dimensional space, then the probability that the particle appears at position x at time t can be obtained from the PDF $|\psi(x,t)|^2$ (Griffith and Schroeter 2018).

In the QPSO, the wave function $\psi(x,t)$ of a particle is obtained by solving the time-independent Schrödinger equation related to a physical particle that moves in a Delta potential well $V(x) = -\gamma\delta(x-\eta)$ with the center η. Consequently, the wave function takes the form as follows:

$$\psi(x) = \frac{1}{\sqrt{L}} e^{-\frac{|x-\eta|}{L}}, \tag{25}$$

where L is the characteristic length of the Delta potential well and e is the natural exponential base. The corresponding PDF of the particle's position in the algorithm is then

$$q(x) = |\psi(x)|^2 = \frac{1}{L} e^{-\frac{2|x-\eta|}{L}}. \tag{26}$$

By employing the Monte Carlo simulation method, one can update the position of the particle according to the following equation:

$$x_j^{(i,\ell+1)} = \eta_j^{(i,\ell)} \pm \frac{L_j^{(i,\ell)}}{2} \ln(1/u_j^{(i,\ell)}), \tag{27}$$

where $x_j^{(i,\ell+1)}$ represents the j-th component of the position of the i-th particle at the $(\ell+1)$-th iteration; $u_j^{(i,\ell)}$ is a random number distributed uniformly within the interval $[0,1]$; $\eta_j^{(i,\ell)}$ is the j-th component of the local attractor of the particle's position and is defined by

$$\eta_j^{(i,\ell)} = \frac{\varphi_j^{(i,\ell)} \mathrm{pbest}_j^{(i,\ell)} + \phi_j^{(i,\ell)} \mathrm{gbest}_j^{(\ell)}}{\varphi_j^{(i,\ell)} + \phi_j^{(i,\ell)}}, \tag{28}$$

where $\varphi_j^{(i,\ell)}$ and $\phi_j^{(i,\ell)}$ are random numbers distributed uniformly within the interval $[0,1]$; The characteristic length $L_j^{(i,\ell)}$ is given as

$$L_j^{(i,\ell)} = 2\alpha \cdot |x_j^{(i,\ell)} - \eta_j^{(i,\ell)}|, \tag{29}$$

where α is the contraction-expansion coefficient controlling the convergence rates of particles.

The control of the characteristic length L is crucial to the convergence performance of the QPSO. In Equation (29), L is determined by the distance between the particle's current position and the local attractor of the particle's position. Although updating L in this way performs well in this study, it may result in unstable convergence for some particles when the population size of the swarm is small. To cope with this problem, Sun et al. (2004b) put forward a variant of the original QPSO, where the vector of the local attractor in Equation (29) is replaced by the mean value of particles' best individual positions. In this study, the update strategy based on Equations (27) ~ (29) is adopted. Other details of the QPSO algorithm can be found in Sun et al. (2012).

4.3 Optimization scheme

To solve the DRBDO problem in Equation (1), the reliability assessment method introduced in Section 3 should be integrated into the QPSO algorithm. Moreover, constraints in the optimization problem should be handled properly, as the QPSO only deals with unconstrained optimization problems. Herein, a penalty-based method is employed. The penalty-based method transfers a constrained optimization problem to an unconstrained one by penalizing infeasible designs during the optimization process (Nocedal and Wright 2006). Accordingly, the unconstrained optimization problem related to the problem in Equation (1) can be constructed as

$$\min_{\boldsymbol{x}} \ \tilde{f}(\boldsymbol{x}) = f(\boldsymbol{x}) \cdot [1 + \beta_p \cdot P(\boldsymbol{x})], \tag{30}$$

where β_p is the penalty coefficient given by $\beta_p = 100 \cdot \ell / N_{\mathrm{It}}$, ℓ is the current iteration number, and N_{It} is the maximum iteration number. The penalty function $P(\boldsymbol{x})$ is defined by

$$P(\boldsymbol{x}) = \sum_{i=1}^{n_{\mathrm{h}}+n_{\mathrm{g}}} \gamma_i \kappa_i(\boldsymbol{x}), \tag{31}$$

where $\kappa_i(\boldsymbol{x})$ represents the violation of the i-th constraint, and γ_i is the weight factor to adjust the penalty for the i-th constraint.

For completeness, the procedures for solving DRBDO problems based on the QPSO and the PDEM are outlined as follows:

Step 1. Initialization: Initialize the QPSO optimizer: the population size N_{p}, the dimension of the position n_x, the maximum iteration number N_{It}, the contraction-expansion coefficient α, particles' positions $\{\boldsymbol{x}^{(i,0)}, i=1,\cdots,N_{\mathrm{p}}\}$, the individual optimal positions of the particles $\{\mathrm{pbest}^{(i,0)}, i=1,\cdots,N_{\mathrm{p}}\}$, and the global optimal position of the particle swarm $\mathrm{gbest}^{(0)}$. Initialize the PDEM solver: the number of the representative points n_{sel}, the distribution parameters of the random variables, and the thresholds related to failure events. Set the iteration index $\ell = 0$.

Step 2. Reliability analysis: Perform the reliability analysis for each particle in $\{\boldsymbol{x}^{(i,\ell)}, i=1,\cdots,N_{\mathrm{p}}\}$ based on the PDEM (refer to Appendix).

Step 3. Evaluation of particles' fitness values: Calculate the fitness value (Equation (30)) of each particle using the penalty-based method.

Step 4. Updating of the optimal solutions: Set the individual optimal positions of the particles and the global optimal position of the swarm as $\{\mathrm{pbest}^{(i,0)}, i=1,\cdots,N_{\mathrm{p}}\}$ and $\mathrm{gbest}^{(0)}$, respectively, if $\ell = 0$; otherwise, update them according to the fitness values at current iteration.

Step 5. Updating of the particles' positions: Update the positions of the particles using Equation (27).

Step 6. Repeating or Ending: Repeat Step 2 ~ Step 4 and set $\ell = \ell + 1$ until the maximum iteration number (adopted in this paper) or the error control criterion is reached.

5 Numerical examples

In this section, numerical examples involving four structural models are presented. The purposes of this work are: (1) to demonstrate the advantages of the PDEM for the reliability analysis and design optimization of stochastic structures; (2) to verify the effectiveness and efficiency of the proposed DRBDO scheme. For these goals, the proposed scheme is employed to optimize a linear truss structure and three nonlinear frame structures under dynamic reliability constraints. The computational consumption of structural reliability analyses based on the PDEM and Monte Carlo simulation (MCS) in the optimization process is compared. In addition, the PSO and the method of moving asymptotes (MMA), a gradient-based optimization algorithm, are also implemented for comparison.

5.1 Example I: A 10-bar linear truss structure

In this example, we are interested in the size optimization of a typical 10-bar truss structure (Li et al. 2007b). The truss is simply supported on the left side and is subjected to point loads suddenly placed at the two free nodes with the constant amplitude of 444.8kN, as shown in Figure 1. Considering the uncertainties in structural parameters, the mass density ρ and the modulus of elasticity E of the material are assumed to be normally-distributed random variables. The probabilistic characterization of the random variables is presented in Table 1. The damping ratios 5% are adopted in the model.

The objective of the design optimization is to minimize the structural weight, and the reliability constraint is to ensure that the first-passage probability of the truss shall not exceed the limit value, $P_F^{\text{th}} = 0.01$. The structure is assumed to be failed if the displacement of any free node of the truss exceeds a prescribed threshold. In this example, the threshold is taken as $u^{\text{th}} = 50.8\text{mm}$. The design variables are the cross-sectional areas of the bars, namely $\boldsymbol{x} = (x_1, \cdots, x_{10})^{\text{T}}$. Therefore, the optimization problem is formulated as

$$\begin{aligned} \min \quad & \sum_{i=1}^{10} x_i l_i \rho \quad , \\ \text{s.t.} \quad & P_F(\boldsymbol{x}) \leqslant P_F^{\text{th}} \\ & x_i \geqslant 64.52\text{mm}^2, i = 1, \cdots, 10 \end{aligned} \tag{32}$$

where l_i is the length of the i-th bar, and ρ is the mass density, which is assumed to be the same for all the bars. The failure probability is defined as

$$P_F(\boldsymbol{x}) = \Pr\left\{ \max_{t \in (0,T]} \left[\max_{r=1,\cdots,8} \left(\left| \frac{u_r(\rho, E, t; \boldsymbol{x})}{u^{\text{th}}} \right| - 1 \right) \right] > 0 \right\}, \tag{33}$$

where u_r stands for the node displacement in the r-th degree of freedom. To obtain structural responses, the Newmark-β method is implemented with the parameters β = 0.25 and γ = 0.5. The failure probability of the structure is estimated through the PDEM (See Appendix) with 300 representative points.

For solving the problem (32), the penalty function mentioned in Equation (30) is defined as

$$P(\boldsymbol{x}) = \begin{cases} 0, & P_F \le P_F^{\text{th}} \\ \dfrac{P_F(\boldsymbol{x}) - P_F^{\text{th}}}{P_F^{\text{th}}}, & P_F > P_F^{\text{th}} \end{cases}. \tag{34}$$

Then the unconstrained optimization problem given by Equation (30) is solved by both the QPSO and the PSO, denoted as Method I (PDEM-QPSO-based method) and Method II (PDEM-PSO-based method), respectively. For comparison, we set three sets of parameters for both methods, including the population size N_{p} and the maximum number of generations N_{It}:

Setting I: $N_{\text{p}} = 10$, $N_{\text{It}} = 500$;

Setting II: $N_{\text{p}} = 20$, $N_{\text{It}} = 300$;

Setting III: $N_{\text{p}} = 30$, $N_{\text{It}} = 200$.

The other parameters are set as follows: for the PSO, $c_1 = c_2 = 0.8$, and $\omega_\ell = 0.9 - 0.5\ell / N_{\text{It}}$, where ℓ is the current iteration number (Li et al. 2007b); for the QPSO, α = 1/0.96. The optimal designs of the linear truss structure are shown in Table 2. The objective function values and the failure probabilities corresponding to the optimal designs are summarized in Table 3, where the means and the standard deviations are related to the individual optimal objective values of all the particles in the swarm.

As seen from Table 3, the differences are relatively small in the final objective function values obtained by Method I (PDEM-QPSO-based method) with different settings, compared with those obtained by Method II (PDEM-PSO-based method). For Method I, even when the population size N_{p} is small, the final objective function values can be satisfactory by increasing the maximum number of generations N_{It}. However, the quality of the results for Method II heavily depends on the population size. Specifically, Method II with small population size (i.e., 10 and 20) tends to be stuck in local optimums. Although the results can be improved by increasing the population size, they are still worse than those obtained by Method I with the same setting. Therefore, it can be concluded that Method I is more robust than Method II with different population sizes.

The data presented in Table 2 further demonstrate the robustness of Method I, as the optimum designs are similar for Method I but quite different for Method II. It should be noted that numerical errors exist in estimating structural failure probability by the numerical procedures of the PDEM. These numerical errors, together with the non-linearity of the reliability constraint function and the random nature of the optimization algorithms, make it impractical to achieve exactly the same solutions for the methods with different settings. From engineering perspective, the differences between the final designs for Method I (shown in Table 2) could be ignored.

From Table 3, it can also be deduced that all particles converge to nearly the same solutions in Method I, while some are prematurely converged in Method II. It is because, in Method I equipped with Setting I or Setting II, the mean value of the individual optimal objective function values is close to the final objective value, while the corresponding standard deviation approaches 0. It is noted although the standard deviation is 7.876 kg in Method I equipped with Setting III, it is negligibly small compared to the corresponding mean value. When the maximum number of generations N_{It} is extended to 500, the standard deviation is close to 0 with the final objective function value of 5790.481 kg (not shown in Table 3). However, that is not the case in Method II.

The iteration history of the objective function value is shown in Figure 2. It is shown that Method I has better convergence performance than Method II (Figure 2 and Table 3). Figure 3 presents the iteration history of the optimization process in terms of the failure probability. It is seen that the first-passage probabilities of the designs are close to 0.01 in the final stage of the optimization, which means the dynamic reliability constraint is active. Moreover, 300 representative points are selected in this example to estimate the failure probabilities of different designs via the PDEM. Therefore, only 300 deterministic structural response analyses are required for a round of reliability analysis.

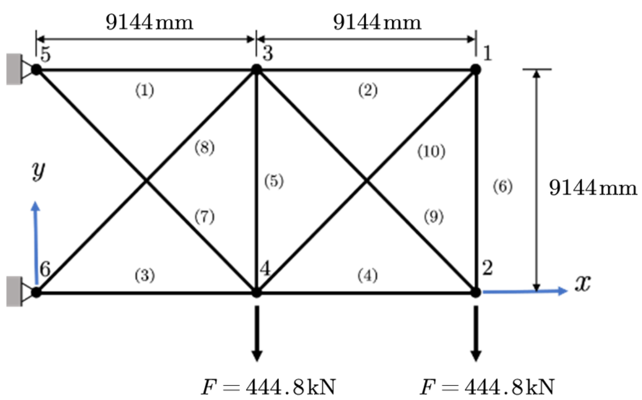

Figure 1. A 10-bar planar truss structure.

Table 1. Probabilistic characterization of the random variables (Example I).

Random variable	Type of distribution	Mean value	Coefficient of variation
ρ	Normal	2.7126 ($\times 10^{-5}$kg/mm^3)	0.10
E	Normal	68,947.5728 (MPa)	0.15

Table 2. Optimum designs (Example I).

Method	N_p	N_{It}	x_1 (mm^2)	x_2 (mm^2)	x_3 (mm^2)	x_4 (mm^2)	x_5 (mm^2)	x_6 (mm^2)	x_7 (mm^2)	x_8 (mm^2)	x_9 (mm^2)	x_{10} (mm^2)
I	10	500	41117	554	40196	26136	65	1336	31718	27783	27588	5712
I	20	300	44157	65	35017	20185	116	1375	17501	30811	34145	8052
I	30	200	41996	140	40811	20206	65	1321	20465	29248	31972	6272
II	10	500	45164	43259	45164	27262	65	13243	38629	29488	21455	17875
II	20	300	45164	7305	45164	19458	12509	102	23574	45164	35734	12831
II	30	200	45164	65	45164	20570	65	65	9626	28791	45164	264

Table 3. Optimum objective function values and corresponding failure probabilities (Example I).

Method	N_p	N_{It}	Objective function			Failure probability
			Value (kg)	Mean (kg)	Standard deviation (kg)	
I	10	500	6090.552	6090.899	0.376	0.01
I	20	300	5793.685	5794.932	0.584	0.01
I	30	200	5794.002	5798.297	7.876	0.01
II	10	500	8253.626	8253.626	0.000	0.01
II	20	300	7481.293	7537.675	134.638	0.01
II	30	200	5812.696	6523.821	864.672	0.01

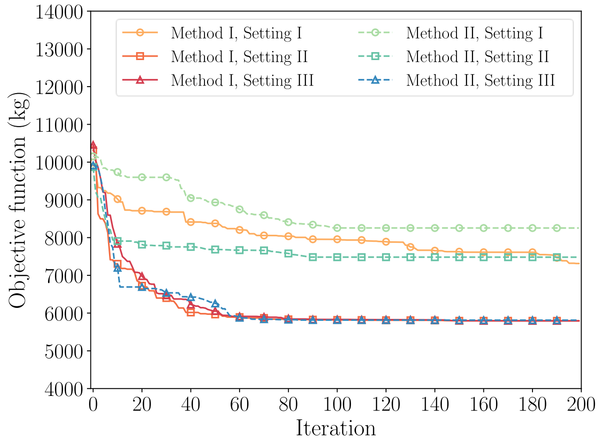

Figure 2. Iteration history in terms of the objective function value (Example I).

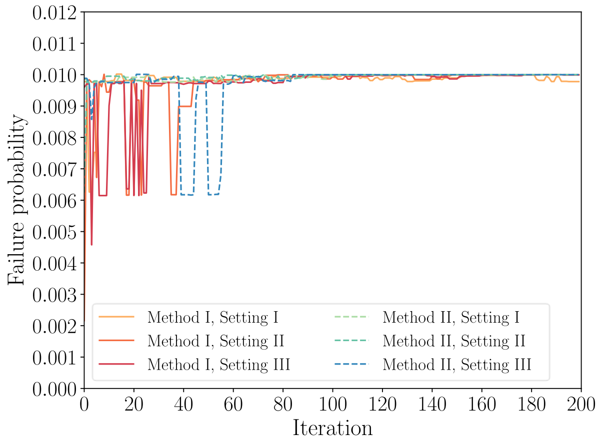

Figure 3. Iteration history in terms of the failure probability (Example I).

5.2 Example II: A 2-DOF hysteretic nonlinear frame structure

In the second example, we consider the design optimization of a 2-storey nonlinear frame structure under earthquake excitations, as shown in Figure 4. The structure is simplified as a 2-degree-of-freedom model with nonlinear restoring force. The floor height of the structure is $h = 3.6\text{m}$. The lumped masses are $m_1 = 1.8 \times 10^5 \text{kg}$ and $m_2 = 1.2 \times 10^5 \text{kg}$. The Rayleigh damping is adopted with the modal damping ratios of 5%. The nonlinear restoring force is formulated with the extended Bouc-Wen model (Ma et al. 2004), whose parameters are presented in Table 4. A typical hysteretic curve of the first floor is shown in Figure 5, demonstrating the strong non-linearity of the structural response.

Uncertainties are involved in the initial lateral stiffnesses of the structure and ground acceleration. In particular, it is assumed that the lateral inter-story stiffnesses $K_i\ (i=1,2)$ of different floors are random variables of independent normal distributions. The mean values $\mu_{K_i}\ (i=1,2)$ of the random variables are taken as the design variables, namely $x_i\ (i=1,2)$. The ground acceleration is assumed to be a random combination of the El Centro acceleration records in the N-S and E-W directions, that is

$$\ddot{u}_g(t) = \Theta_1 \ddot{u}_{g,\mathrm{NS}}(t) + \Theta_2 \ddot{u}_{g,\mathrm{EW}}(t), \tag{35}$$

where $\ddot{u}_{g,\mathrm{NS}}(t)$ and $\ddot{u}_{g,\mathrm{EW}}(t)$ are the El Centro acceleration records in the N-S and E-W directions, respectively; Θ_1 and Θ_2 are the random combination coefficients. The probability information of the random variables is listed in Table 5, where g is the gravitational acceleration, i.e., g=9.807m/s^2. Totally, there are four random variables involved in the example.

The design optimization aims at minimizing structural cost, which is assumed to be proportional to the lateral inter-story stiffnesses of the structure. Thus, the objective function is formulated as the sum of all the lateral inter-story stiffnesses (Chen et al. 2020). Considering structural performance requirements, the stiffness of the lower floor is required to be greater than that of the upper one. The structure is considered to fail when any inter-story drift exceeds a specified threshold, and the corresponding failure probability is defined as

$$P_F(x_1,x_2) = \Pr\left\{ \max_{t\in(0,T]} \left[\max_{r=1,2} \left[\left| z_r(\boldsymbol{\Theta},t)/(h_r/250) \right| \right] \right] > 1 \right\}, \tag{36}$$

where $z_r(\boldsymbol{\Theta},t)$ is the inter-story drift of the r-th floor; $\boldsymbol{\Theta} = (K_1, K_2, \Theta_1, \Theta_2)^{\mathrm{T}}$ is the random vector; h_r is the height of the r-th floor of the structure; and T is the duration of the ground acceleration. The design optimization problem is formulated as

$$\begin{aligned} \min \quad & f(x_1,x_2) = x_1 + x_2 \\ \text{s.t.} \quad & g(x_1,x_2) = x_2 - x_1 \le 0 \\ & h(x_1,x_2) = P_F(x_1,x_2) - P_F^{\mathrm{th}} \le 0 \\ & 0.5\times10^8\,\mathrm{N\cdot m^{-1}} \le x_1 \le 1.2\times10^8\,\mathrm{N\cdot m^{-1}} \\ & 0.3\times10^8\,\mathrm{N\cdot m^{-1}} \le x_2 \le 1.0\times10^8\,\mathrm{N\cdot m^{-1}}, \end{aligned} \tag{37}$$

where $P_F^{\mathrm{th}} = 0.01$ is the threshold of the failure probability.

To evaluate the failure probability of the structure by the PDEM, 300 representative points are selected. Note that the representative points should be updated at each iteration step. It is because the mean values of the random variables are the design variables. Consequently, the changes in the design variables affect the joint probability distribution of all the random variables. Figure 6 shows the failure probability curve obtained by the PDEM and MCS. The number of samples for MCS is 10000. It is seen that the PDEM accords well with MCS, but the number of deterministic structural analyses involved in the PDEM is much less than that involved in MCS. When the PDEM and MCS are employed in the DRBDO, the numbers of the structural analyses for the PDEM and MCS are

$300 \times N_{\mathrm{It}} \times N_{\mathrm{p}}$ and $10000 \times N_{\mathrm{It}} \times N_{\mathrm{p}}$, respectively. Therefore, the PDEM can significantly reduce the computational efforts for solving DRBDO problems.

The optimization problem defined in Equation (37) is also solved by Method I (PDEM-QPSO-based method) and Method II (PDEM-PSO-based method). The constraints in the problem are dealt with using the penalty-based method introduced in Section 4.3. In order to investigate the performance of the Method I and Method II, three sets of parameters are considered for solving the problem:

Setting I: $N_{\mathrm{p}} = 10$, $N_{\mathrm{It}} = 300$;

Setting II: $N_{\mathrm{p}} = 20$, $N_{\mathrm{It}} = 300$;

Setting III: $N_{\mathrm{p}} = 30$, $N_{\mathrm{It}} = 300$.

We have three trial runs for every setting to take into account the randomness of the optimization algorithms. The other parameters are the same as those in Example I.

The iteration histories of the average objective function and the average design variables are shown in Figure 7 and Figure 8, respectively. It is observed that significant updates of the design variables occur mainly in the first 50 iterations of the optimization process. In this stage, the decreasing rates of the objective function values of both Method I and Method II are slightly improved as the population size N_{p} increases. Although the objective function value of Method I declines more slowly than Method II when the population size N_{p} equals 10, the former is smaller than the latter after about 130 iterations. It can be attributed to the better ability of the QPSO algorithm to explore the whole design space. On the other hand, since there are only two design variables, both methods converge quickly despite the non-linearity of the reliability constraint function complicating the optimization problem. In the later stages of the optimization, the changes in the design variables are essentially controlled by numerical errors in evaluating structural failure probability. However, the slight differences between optimization results are negligible from the engineering point of view. The average results of the optimization are presented in Table 6. It is seen that the optimal designs and the corresponding objective function values obtained by Method I with different settings are almost identical. However, for Method II, the result with the small population size $N_{\mathrm{p}} = 10$ is slightly worse than the others. In this sense, Method I performs better than Method II. Moreover, the failure probabilities of all the final designs are equal to the prescribed threshold of 0.01, which emphasizes the necessity of considering reliability constraints in the optimization process.

To gain more insight into the effectiveness of the proposed scheme, the problem (37) is also solved by MMA (Svanberg 1987) for comparison. MMA is a gradient-based optimization algorithm extensively used for structural design optimization. In MMA, at every iteration, a convex approximation of the original problem is constructed around the current design and then is solved to improve the current design. The readers are referred to Svanberg (2007) for more details of the algorithm. To construct the sub-problem, the gradients of the objective function and the constraint function with respect to the design variables are required. Since the analytical gradient of the reliability constraint function is unavailable, it is calculated using the finite difference method in this study. Three feasible designs are adopted as initial solutions: $\boldsymbol{x}_{\text{init},1} = (1.0,1.0)^{\text{T}}$ $(\times 10^{8}\,\text{N}\cdot\text{m}^{-1})$, $\boldsymbol{x}_{\text{init},2} = (1.2,1.0)^{\text{T}}$ $(\times 10^{8}\,\text{N}\cdot\text{m}^{-1})$ and $\boldsymbol{x}_{\text{init},3} = (1.2,0.8)^{\text{T}}$ $(\times 10^{8}\,\text{N}\cdot\text{m}^{-1})$.

Table 7 presents the final objective function values, the final design variables and the corresponding failure probabilities of the problem. It is seen that the results obtained by MMA are affected by the initial designs and the step sizes of the finite difference method. The final designs are all infeasible, except for the case where the initial design and the step size are $\boldsymbol{x}_{\text{init},2} = (1.2,1.0)^{\text{T}}$ $(\times 10^{8}\,\text{N}\cdot\text{m}^{-1})$ and 0.010, respectively. However, the only feasible design is not the solution to the problem. The poor performance of the gradient-based algorithm in this example may be attributed to the presence of the reliability constraint. On the one hand, the reliability constraint intensifies the non-linearity and non-convexity of the problem, as shown in Figure 9. On the other hand, the gradient of the reliability constraint obtained by the finite difference method is impossible to be exact, which increases the probability of the algorithm obtaining a local optimum or failing to converge. In this context, the proposed method is preferable for solving this type of DRBDO problems.

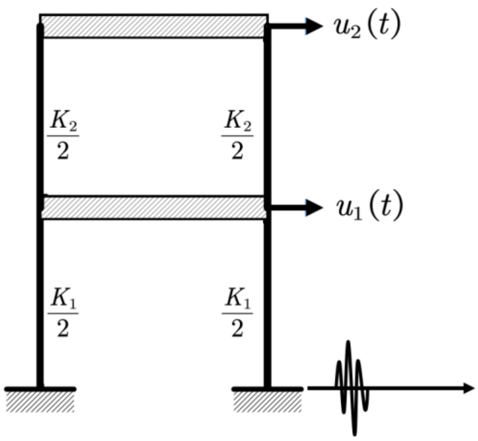

Figure 4. A 2-storey frame structure.

Table 4. The parameters for Bouc-Wen model.

α^{bw}	A^{bw}	β^{bw}	γ^{bw}	n^{bw}	d_{ν}^{bw}	d_{η}^{bw}	p^{bw}	q^{bw}	ψ^{bw}	λ^{bw}	d_{ψ}^{bw}	ζ_{s}^{bw}
0.04	1	320	150	1	300	300	1000	0.25	0.05	0.5	5	0.99

Table 5. Probabilistic characterization of the random variables (Example II).

Random variable	Type of distribution	Mean value	Coefficient of variation
K_1	Normal	$x_1 = \mu_{K_1}$	0.05
K_2	Normal	$x_2 = \mu_{K_2}$	0.05
Θ_1	Normal	0.10 g	0.10
Θ_2	Normal	0.10 g	0.10

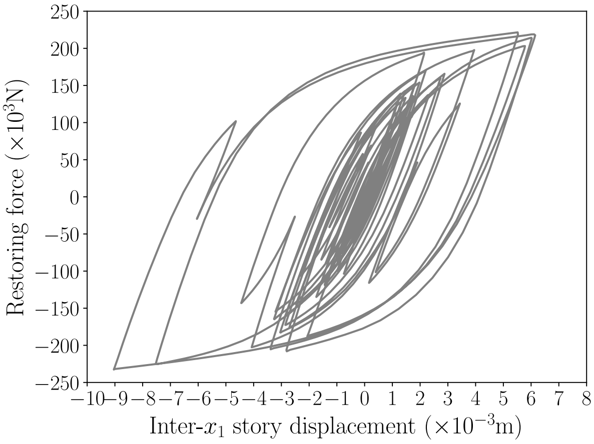

Figure 5. A typical hysteretic curve.

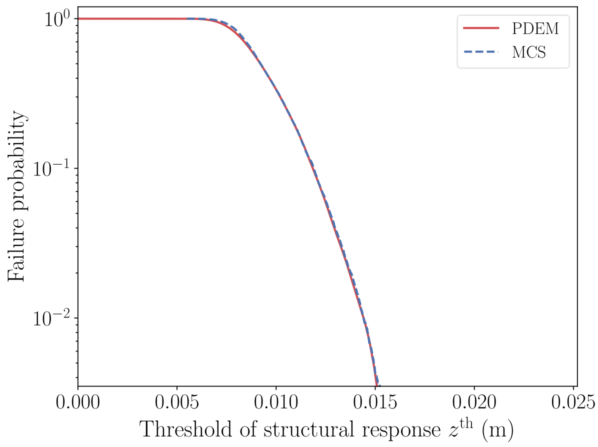

Figure 6. Probability of failure estimates obtained by different methods.

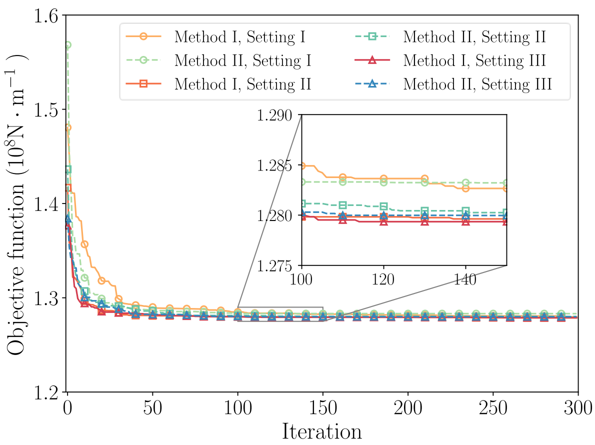

Figure 7. Iteration history in terms of the objective function value (Example II).

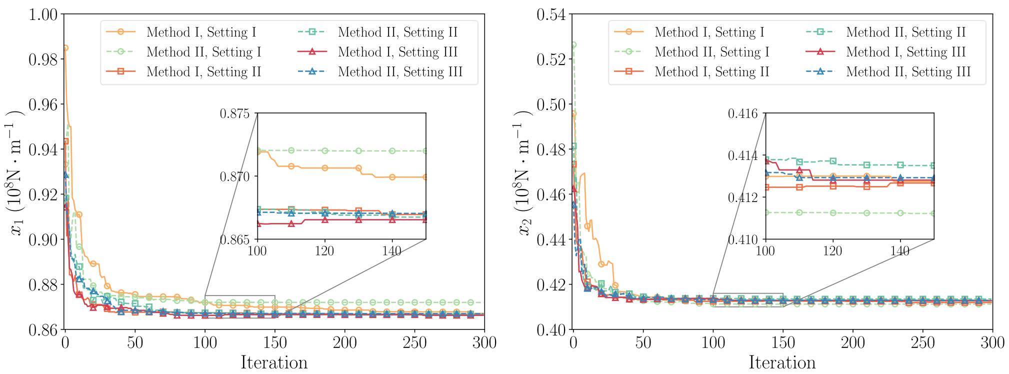

Figure 8. Iteration histories in terms of the design variable (Example II).

Table 6. Average optimum results for different settings (Example II).

Method	Population size	Objective function value ($\times 10^8\,\mathrm{N \cdot m^{-1}}$)	x_1 ($\times 10^8\,\mathrm{N \cdot m^{-1}}$)	x_2 ($\times 10^8\,\mathrm{N \cdot m^{-1}}$)	Failure probability
I	10	1.280	0.867	0.413	0.01
I	20	1.279	0.867	0.412	0.01
I	30	1.279	0.866	0.413	0.01
II	10	1.283	0.872	0.411	0.01
II	20	1.280	0.867	0.414	0.01
II	30	1.280	0.867	0.413	0.01

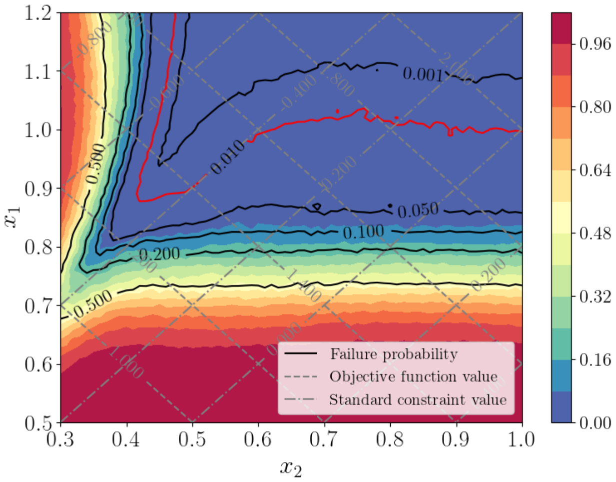

Figure 9. Contour of the failure probability (Example II).

Table 7. Optimization results obtained by MMA (Example II).

$\boldsymbol{x}_{\mathrm{init}}$ ($\times 10^8\,\mathrm{N \cdot m^{-1}}$)	Step size of the finite difference	Objective function value ($\times 10^8\,\mathrm{N \cdot m^{-1}}$)	x_1 ($\times 10^8\,\mathrm{N \cdot m^{-1}}$)	x_2 ($\times 10^8\,\mathrm{N \cdot m^{-1}}$)	Failure probability
$(1.0,1.0)^{\mathrm{T}}$	0.001	1.109	0.765	0.344	0.162
$(1.2,1.0)^{\mathrm{T}}$	0.001	1.067	0.726	0.341	0.319
$(1.2,0.8)^{\mathrm{T}}$	0.001	1.046	0.737	0.309	0.340
$(1.0,1.0)^{\mathrm{T}}$	0.010	1.246	0.848	0.398	0.026
$(1.2,1.0)^{\mathrm{T}}$	0.010	2.063	1.200	0.863	0.000
$(1.2,0.8)^{\mathrm{T}}$	0.010	1.368	0.861	0.507	0.029

5.3 Example III: A 10-DOF hysteretic nonlinear frame structure

In the third case, the design optimization of a 10-storey nonlinear frame structure is considered. The model of the frame structure is shown in Figure 10. All the floor heights of the structure are $h = 3.6\text{m}$, except for the ground floor height being 4.0 m. The lumped masses from bottom to top are 3.4, 3.4, 3.2, 3.2, 3.2, 2.8, 2.8, 2.8, 2.6 and 2.6 $(\times 10^5 \text{kg})$, respectively. The modal damping ratios are 5%. The extended Bouc-Wen model with the parameters presented in Table 4 is also adopted to describe the nonlinear behavior of the structure.

The structure is subjected to the earthquake excitation defined as Equation (35), where Θ_1 and Θ_2 are the random combination coefficients following normal distributions. The lateral inter-story stiffnesses of different floors $K_i\ (i = 1, \cdots, 10)$ are assumed to be normally distributed random variables, whose mean values $\mu_{K_i}\ (i = 1, \cdots, 10)$ are taken as the design variables, namely $x_i\ (i = 1, \cdots, 10)$. The probabilistic description of all the random variables in this example is listed in Table 8.

The objective of this design problem is to minimize the total lateral inter-story stiffness of the structure. The performance requirements and the reliability constraint of the structure are identical to those in Example II. Therefore, the optimization problem is formulated as

$$\begin{aligned} \min \quad & f(\boldsymbol{x}) = \sum_{i=1}^{10} x_i \\ \text{s.t.} \quad & g_j(\boldsymbol{x}) = x_{j+1} - x_j \le 0, \quad j = 1, 2, \cdots, 9 \\ & h(\boldsymbol{x}) = P_F(\boldsymbol{x}) - P_F^{\text{th}} \le 0 \\ & 5 \times 10^8\,\text{N} \cdot \text{m}^{-1} \le x_i \le 15 \times 10^8\,\text{N} \cdot \text{m}^{-1}, \quad i = 1, \cdots, 10 \end{aligned} \quad , \tag{38}$$

where the threshold of the failure probability P_F^{th} is set as 0.01, and the failure probability of the structure is

$$P_F(\boldsymbol{x}) = \Pr\left\{ \max_{t \in (0,T]} \left[\max_{r=1,\cdots,10} \left[\left| z_r(\boldsymbol{\Theta}, t; \boldsymbol{x}) / (h_r / 250) \right| \right] \right] > 1 \right\}, \tag{39}$$

where $z_r(\boldsymbol{\Theta}, t)$ is the inter-story drift of the r-th floor; $\boldsymbol{\Theta} = (K_1, \cdots, K_{10}, \Theta_1, \Theta_2)^{\text{T}}$ is the vector of random variables.

The optimization problem in Equation (38) is solved by both Method I (PDEM-QPSO-based method) and Method II (PDEM-PSO-based method). All parameters and settings are the same as in those Example II, except those mentioned later. The number of the representative points for the PDEM is set as 700.

The final designs obtained by different methods with different settings are shown in Table 9. Figure 11 presents the iteration history of the objective function value. It is seen that in all the settings, Method I achieves nearly the same solutions, while Method II always obtains premature designs despite having a faster convergence rate. Note that increasing the population size cannot monotonically improve the performance of Method II. In particular, Method II with the large population size (N_p =20) finally yields a design inferior to that with the small population size (N_p =10). This indicates the stability of Method I in a sense. Together with the results of Example II, it can also be deduced that the superiority of Method I will be more evident as the number of design variables increases.

To take into account the randomness of the optimization algorithms, both Method I and Method II equipped with Setting II are run twice. The iteration history of the average objective function is shown in Figure 12, and the corresponding results are presented in Table 10. It is shown that Method II is premature in the early stage of the optimization, while Method I progresses well until finding the solution. Note that although the strong non-linearity of the structure and the increase in the number of the design variables complicate the optimization problem, it can be well solved using Method I (with different settings). Thus, the results of this example again substantiate the effectiveness of the proposed scheme.

The problem (38) is also solved by MMA. The optimization algorithm is initialized with three initial solutions, namely $\boldsymbol{x}_{\mathrm{init},1} = (8,8,8,8,8,8,8,8,8,8)^\mathrm{T}\ (\times 10^8\,\mathrm{N}\cdot\mathrm{m}^{-1})$, $\boldsymbol{x}_{\mathrm{init},2} = (10,10,10,10,10,10,10,10,10,10)^\mathrm{T}\ (\times 10^8\,\mathrm{N}\cdot\mathrm{m}^{-1})$ and $\boldsymbol{x}_{\mathrm{init},3} = (15,15,15,15,15,15,15,15,15,15)^\mathrm{T}$ $(\times 10^8\,\mathrm{N}\cdot\mathrm{m}^{-1})$, with a consistent step size of 0.05 for the finite difference. The optimization results presented in Table 11 show that MMA fails to yield feasible solutions for the three cases, revealing the limitations of the gradient-based optimization algorithm for this type of problems. In fact, as the design space for the problem expands exponentially with an increasing number of design variables, the number of local optima can increase significantly. Moreover, the numerical solution of the structural response and dynamic reliability may induce numerical non-convexity and therefore result in the non-smooth characteristics of the feasible domain boundary (Taflanidis and Beck, 2008). These factors can collectively contribute to the suboptimal performance of MMA. To achieve a more profound comprehension of this issue, the projection of the failure probability surface and its contour in dimensions x_1 and x_2 is demonstrated in Figure 13, with the other dimensions fixed at $(x_3, x_4, \cdots, x_{10}) =$ (9., 8., 7.5, 6.5, 5.5, 5, 5, 5) $(\times 10^8\,\mathrm{N}\cdot\mathrm{m}^{-1})$. It is evident that the contour exhibits a high degree of non-linearity and non-convexity. Although the non-convexity of the failure probability surface is visually confirmed in two dimensions, it can be easily deduced based on the definition of convexity that the original high-dimensional surface of the failure probability is also non-convex. Therefore, solving the optimization problem may be a formidable challenge for the gradient-based algorithm. Moreover, the irregularity of the failure probability contour induced by the numerical calculation can further exacerbate the challenge. In comparison, the proposed scheme (Method I) demonstrates superior performance, which can be attributed to the global convergence of the QPSO. Sun et al. (2019) have proven the QPSO algorithm asymptotically converges to the global optimum with probability one based on the theory of the absorbing discrete Markov model. Theoretically, the QPSO is more likely to escape local optima and converge towards the global optimum as the optimization progresses. This feature endows the proposed scheme with a stable optimization ability, even in the presence of non-convexity in the optimization problem.

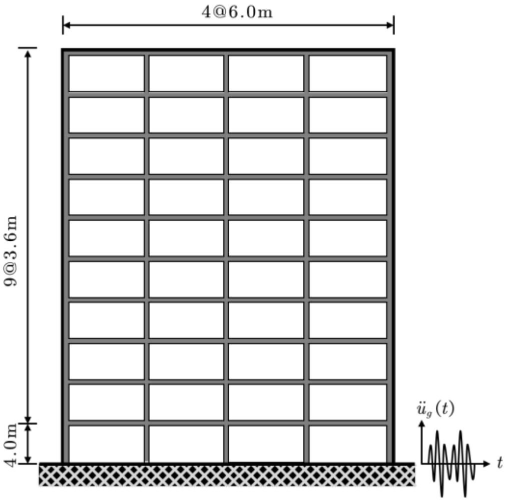

Figure 10. A 10-storey frame structure.

Table 8. Probabilistic characterization of the random variables (Example III).

Random variable	Type of distribution	Mean value	Coefficient of variation
$K_i\,(i=1,\cdots,10)$	Normal	$x_i=\mu_{K_i}$	0.10
$\Theta_i\,(i=1,2)$	Normal	0.10 g	0.15

Table 9. Optimum designs and corresponding objective function values (Example III)*.

Method	N_{p}	Objective function value	x_1	x_2	x_3	x_4	x_5	x_6	x_7	x_8	x_9	x_{10}
I	10	69.340	9.638	9.362	8.669	7.885	7.256	6.189	5.243	5.008	5.010	5.006
I	20	68.943	9.553	9.157	8.508	7.788	7.441	6.164	5.321	5.010	5.000	5.000
I	30	69.245	9.814	9.134	8.584	7.942	7.323	6.244	5.201	5.003	5.000	5.000
II	10	96.913	12.215	11.862	11.596	11.652	11.654	10.261	10.275	7.093	5.000	5.000
II	20	106.183	12.406	11.226	10.536	10.799	9.460	12.711	7.732	10.415	8.164	11.136
II	30	88.456	11.230	11.235	10.464	10.444	8.348	8.345	8.344	7.135	7.102	5.769

*The units of the objective function value and the design variables $x_i\ (i=1,\cdots,10)$ are $\times 10^8\,\mathrm{N}\cdot\mathrm{m}^{-1}$.

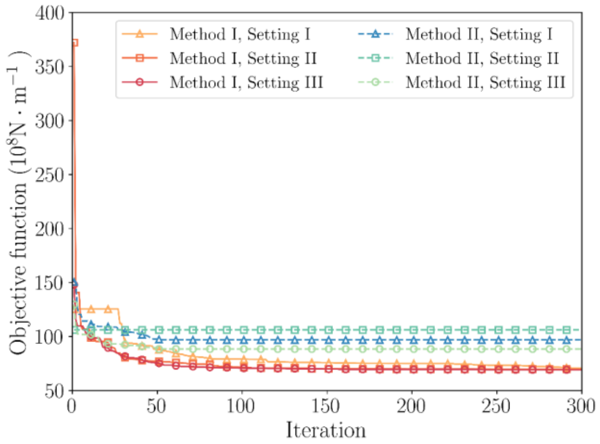

Figure 11. Iteration history in terms of the objective function value (Example III).

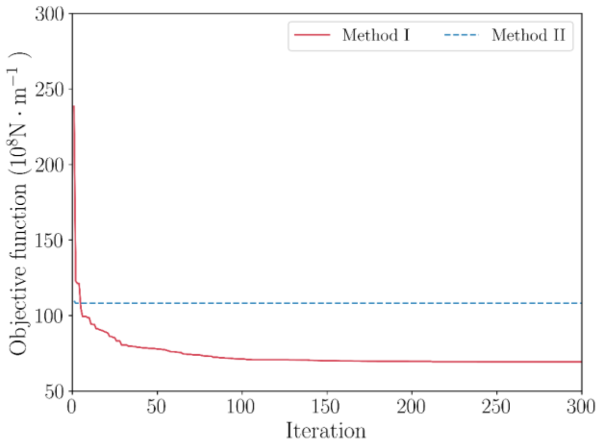

Figure 12. Iteration history in terms of the average objective function value

(Example III, $N_p = 20$).

Table 10. Average optimum designs and corresponding objective function values (Example III) *.

Method	Objective function value	x_1	x_2	x_3	x_4	x_5	x_6	x_7	x_8	x_9	x_{10}
I	69.325	9.802	9.476	8.542	7.813	7.257	6.119	5.300	5.014	5.000	5.000
II	108.127	12.119	11.528	10.570	12.365	9.732	10.233	7.076	10.189	10.265	11.602

*The units of the objective function value and the design variables x_i $(i = 1, \cdots, 10)$ are $\times 10^8\,\mathrm{N \cdot m^{-1}}$.

Table 11. Optimization results obtained by MMA (Example III).

Initial solution	Objective function value ($\times 10^8\,\mathrm{N \cdot m^{-1}}$)	$\boldsymbol{x}_{\mathrm{init}}$ ($\times 10^8\,\mathrm{N \cdot m^{-1}}$)	Failure probability
$\boldsymbol{x}_{\mathrm{init},1}$	56.281	$(7.006, 6.570, 6.306, 5.891, 5.508, 5.000, 5.000, 5.000, 5.000, 5.000)^{\mathrm{T}}$	0.023
$\boldsymbol{x}_{\mathrm{init},2}$	57.258	$(7.210, 6.734, 6.568, 6.065, 5.681, 5.000, 5.000, 5.000, 5.000, 5.000)^{\mathrm{T}}$	0.022
$\boldsymbol{x}_{\mathrm{init},3}$	56.722	$(7.121, 6.563, 6.497, 5.928, 5.614, 5.000, 5.000, 5.000, 5.000, 5.000)^{\mathrm{T}}$	0.023

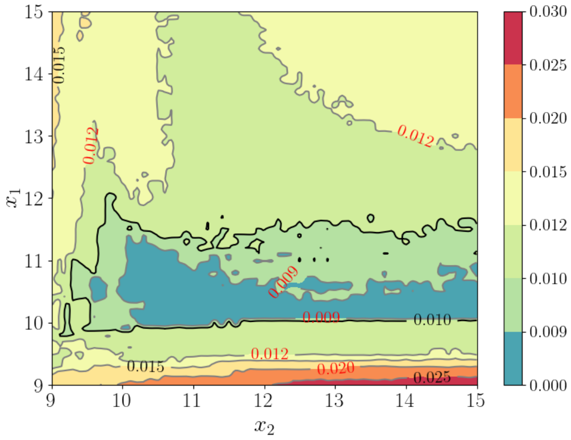

Figure 13. Contour of the failure probability (Example III).

5.4 Example IV: A 20-DOF hysteretic nonlinear frame structure

This example involves the optimization of a 20-storey frame structure to further investigate the effectiveness and applicability of the proposed scheme under varying numbers of design variables and constraints. The structure is shown in Figure 14. The lumped masses of the structure from bottom to top are 2.6, 2.4, 2.2, 2.0, 2.0, 2.0, 2.0, 2.0, 2.0, 2.0, 2.0, 2.0, 2.0, 2.0, 2.0, 2.0, 2.0, 2.0, 2.0 and 1.8 $(\times 10^5\mathrm{kg})$, respectively. Except for the following details, the remaining information is the same as that of Example III.

The lateral inter-story stiffnesses of the structure and the combination coefficients of the amplitude of the El Centro acceleration are taken as random variables, with the corresponding probability information provided in Table 12. To accommodate different numbers of design variables, the mean values of the lateral inter-story stiffnesses are linked to 2, 5, 10, and 20 design variables, respectively. The details of the linkage are provided in Table 13, where n_x denotes the number of design variables. The optimization objective and the reliability constraint in this example are the identical to those in Example III, while the standard constraints are established in two ways: either by taking all the performance requirements into account or by excluding them. Consequently, a total of eight optimization cases are set in this example.

The optimization problems are solved by the proposed scheme with the population size $N_{\mathrm{p}} = 20$ and the maximum number of generations $N_{\mathrm{It}} = 300$. The objective function values at the final designs and the corresponding failure probabilities for all the cases are presented in Table 14. The results demonstrate that increasing the number of design variables n_x can heighten the intricacy of the optimization. For the cases where the structural performance requirements should be met, the proposed scheme can achieve satisfactory results when n_x is small (ID 2 & ID 4). As n_x increases, it becomes crucial to appropriately handle the constraints; otherwise, the optimization algorithm may get stuck in the early stages of the optimization process (ID 8). In this example, two techniques are employed to deal with the performance requirements, namely reducing the penalty associated with the constraints (ID 6) and forcing all the updated design variables to satisfy the performance requirements during the optimization process (ID 9). For the cases where the structural performance requirements are not imposed, the proposed scheme tends to converge to the solutions more readily (ID 1, ID 3 & ID 5). However, the performance of the optimization algorithm may become somewhat unstable as n_x increases, which indicates that repetitive execution of the optimization can yield solutions that are either satisfactory (ID 7) or of poor quality. To mitigate the instability, it is advisable to improve the initial solutions, for example, by ensuring they are all feasible.

On the other hand, it is observed that the objective function value tends to decrease as the number of design variables increases. This trend can be attributed to the linking of design variables, as it constrains the design space and consequently filters out some superior designs. Nevertheless, the extent of the decline in the objective function value is limited. Therefore, when performing structural optimization for engineering applications, it is meaningful to determine an appropriate number of design variables to strike a balance between the computational complexity and the quality of the design. Furthermore, an increase in the standard deviation of the optimal objective function value indicates a larger number of particles prematurely converging as the number of design variables grows. This highlights the potential risk of premature convergence when the number of design variables is increased.

To measure the optimization efficiency, the variation of the objective function is defined by

$$c_{\mathrm{err}} = \left[\left| \sum_{i=1}^{N_0} (\tilde{f}_{\ell-i+1} - \tilde{f}_{\ell-N_0-i+1}) \right| \right] / \sum_{i=1}^{N_0} \tilde{f}_{\ell-i+1} \tag{40}$$

where ℓ is the number of current design iteration and N_0 is a constant equal to 5. Figure 15 presents the history of the variation of the objective function value c_{err}. It is observed that the objective function rapidly achieves a stationary state when the number of design variables is small, regardless of the presence of performance requirements. In contrast, increasing the number of design variables can result in a prolonged duration for the objective function to attain the stability. Furthermore, the consideration of the performance constraints may further increase this duration. However, it should be noted that this observation is not applicable to the case where the performance constraints are considered with $n_x = 20$, as seen in Figure 15(b). In this case, the variation of the objective function value remains constant due to the algorithm's inability to update the design variables. This inability underscores the complexity of the optimization problems involving multiple constraints and design variables.

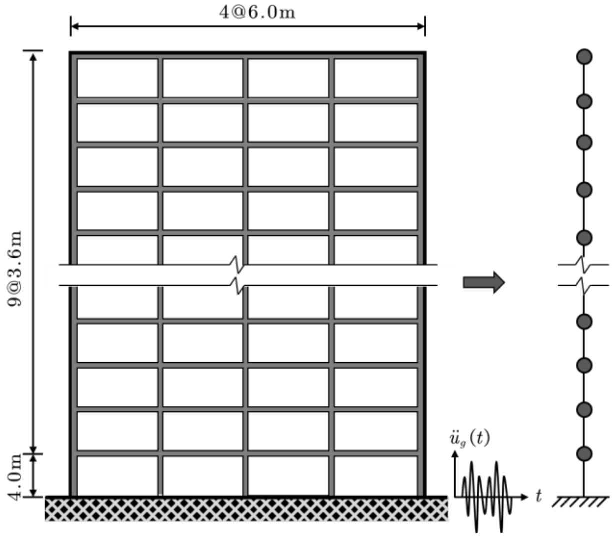

Figure 14. A 20-storey frame structure.

Table 12. Probabilistic characterization of the random variables (Example IV).

Random variable	Type of distribution	Mean value	Coefficient of variation
$K_i\,(i=1,\cdots,20)$	Normal	$x_i = \mu_{K_i}$	0.10
$\Theta_i\,(i=1,2)$	Normal	0.10 g	0.15

Table 13. Scenarios for the linkage of the design variables (Example IV) *.

n_x	Design variables	Description of x_i
2	$\{x_i \mid x_i = \mu_{K,10i-9} = \cdots = \mu_{K,10i}\}(i=1,2)$	The mean value of the lateral stiffnesses of the $(10i-9)$-th to $(10i)$-th floors.
5	$\{x_i \mid x_i = \mu_{K,4i-3} = \cdots = \mu_{K,4i}\}(i=1,\cdots,5)$	The mean value of the lateral stiffnesses of the $(4i-3)$-th to $(4i)$-th floors.
10	$\{x_i \mid x_i = \mu_{K,2i-1} = \cdots = \mu_{K,2i}\}(i=1,\cdots,10)$	The mean value of the lateral stiffnesses of the $(2i-1)$-th to $(2i)$-th floors.
20	$\{x_i \mid x_i = \mu_{K,i}\}(i=1,\cdots,20)$	The mean value of the lateral stiffness of the i-th floor.

*The units of the design variables x_i $(i=1,\cdots,n_x)$ are $\times 10^8\,\mathrm{N\cdot m^{-1}}$.

Table 14. Optimization results (Example IV) *.

ID	n_x	Performance requirements	Objective function		
			Value	Mean	Standard deviation
1	2	None	122.36	122.58	0.16
2		All	122.75	122.86	0.08
3	5	None	89.88	90.11	0.67
4		All	89.76	89.89	0.07
5	10	None	85.06	188.66	316.09
6		All	86.73	168.33	353.73
7	20	None	85.81	368.98	880.46
8		All	583.58	2194.47	1075.57
9		All	82.85	88.94	12.91

*The units of the objective function value, mean, and standard deviation are $\times 10^8\,\mathrm{N\cdot m^{-1}}$.

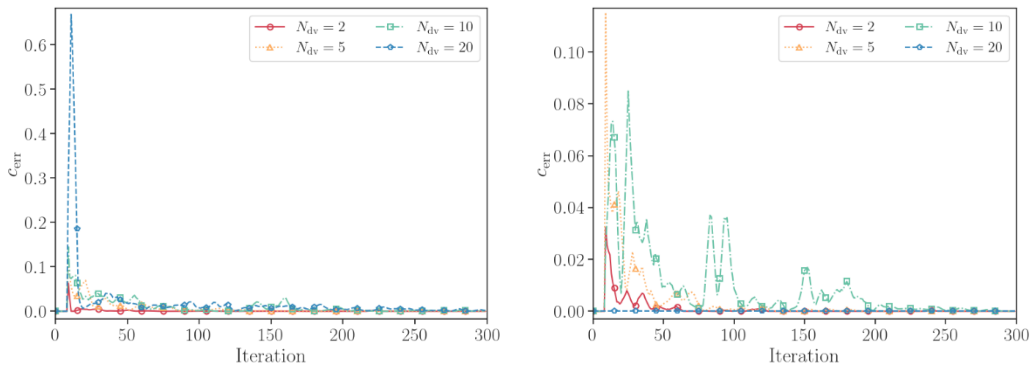

(a) (b)

Figure 15. History of the variation of the objective function: (a) without the performance constraints; (b) with the performance constraints (Example IV).

6 Conclusions

A general scheme for solving a class of DRBDO problems has been proposed. The problem is formulated as a standard minimization problem characterized by dynamic reliability constraints. The quantum particle swarm algorithm is adopted to solve the problem. During the optimization process, structural dynamic reliability is estimated using the PDEM. To the authors' knowledge, this is the first application of quantum-inspired algorithms to the field of design optimization for dynamical systems under uncertainties.

Several examples concerning linear and nonlinear stochastic systems subjected to dynamic excitations are carried out to verify the effectiveness and applicability of the proposed scheme. Some concluding remarks include:

(1) The PDEM is highly efficient and accurate in evaluating the dynamic reliability of complex nonlinear structures. When integrated into the DRBDO scheme, it can significantly promote the efficiency of the optimization.

(2) The proposed DRBDO scheme can deal with optimization problems involving stochastic dynamical structures with strong nonlinear behaviors. Such problems typically exhibit high level of non-linearity and non-convexity, and may be devoid of analytical gradient information related to reliability constraints. Consequently, they can be intractable for gradient-based algorithms, which work well in general when the objective function is smooth and differentiable or when the gradient information can be efficiently calculated. In this context, the proposed scheme is both practical and advantageous, as demonstrated by the numerical examples.

(3) The proposed scheme offers a swifter convergence rate and more robust convergence capacity, compared with the DRBDO scheme that employs the classical PSO algorithm. Evaluating structural dynamic reliability is commonly computationally intensive, which consequently complicates the trial-and-error process for solving DRBDO problems. In this regard, the characteristics of the proposed scheme are crucial in effectively obtaining solutions.

(4) The proposed scheme proves to be effective and efficient when the numbers of the design variables and the constraints are relatively small. However, an increase in the number of the constraints can result in a convoluted and irregular feasible domain, which makes it challenging for the optimization algorithm to locate feasible solutions and may lead to premature convergence. Similarly, an increase in the number of design variables can significantly expand the design space, resulting in a more complex reliability contour

surface, which further complicates the optimization process. These factors can worsen the convergence performance of the proposed scheme. To overcome these challenges, it is essential to adopt appropriate techniques to handle the multiple constraints and improve the quality of the initial solutions.

Future research efforts include further improving the performance of the proposed scheme and applying the proposed scheme to optimize more complicated stochastic structures. Solving the DRBDO problems involving discrete (or mixed) design variables is another research direction. The investigation in these directions is currently underway.

7 Acknowledgements

The financial support from the National Natural Science Foundation of China (the National Distinguished Youth Fund of NSFC with Grant No. 51725804 and the NSFC-Guangdong Province Joint Project Grant No. U1711264) is highly appreciated.

8 Appendix. Numerical procedures for the PDEM

In general, the numerical procedures for solving the GDEE (Equation (8)-(9) and Equation(19)-(20)) are as follows:

Step A.1: Select a representative point set $M_{n_{\mathrm{sel}}} = \left\{(\boldsymbol{\theta}_q, P_q)\right\}_{q=1}^{n_{\mathrm{sel}}}$ in the probability space associated with random vector $\boldsymbol{\Theta}$ using the generalized F-discrepancy minimization-based point selection strategy (Chen et al. 2016), where n_{sel} is the number of the representative points, $\boldsymbol{\theta}_q$ is the q-th representative point with a representative region $\Omega_{\boldsymbol{\Theta}_q}$, and P_q is the assigned probability of $\boldsymbol{\theta}_q$ given by

$$P_q = \int_{\Omega_{\boldsymbol{\Theta}_q}} p_{\boldsymbol{\Theta}}(\boldsymbol{\theta})\,\mathrm{d}\boldsymbol{\theta}\,. \tag{41}$$

Step A.2: Carry out deterministic structural analysis for each representative point $\boldsymbol{\theta}_q, q = 1,\cdots,n_{\mathrm{sel}}$ to capture the velocity responses $\dot{Z}(\boldsymbol{\theta}_q, t; \boldsymbol{x})$ or $\dot{W}(\boldsymbol{\theta}_q, \tau; \boldsymbol{x}), q = 1,\cdots,n_{\mathrm{sel}}$.

Step A.3: Substitute $\dot{Z}(\boldsymbol{\theta}_q, t; \boldsymbol{x})$ or $\dot{W}(\boldsymbol{\theta}_q, \tau; \boldsymbol{x})$ into the GDEE (Equation (8) or Equation(19)) and solve the GDEE under the initial condition (Equation (9) or Equation (20)) with the finite difference method for each representative point $\boldsymbol{\theta}_q, q = 1,\cdots,n_{\mathrm{sel}}$, yielding the numerical solutions $p_{Z\boldsymbol{\Theta}}(z, \boldsymbol{\theta}_q, t; \boldsymbol{x})$ or $p_{W\boldsymbol{\Theta}}(w, \boldsymbol{\theta}_q, \tau; \boldsymbol{x})$, $q = 1,\cdots,n_{\mathrm{sel}}$.

Step A.4: Take numerical integration in Equation (10) or Equation (21) to obtain the PDF of the structural response of interest, that is

$$p_Z(z,t;\boldsymbol{x}) = \int_{\Omega_{\boldsymbol{\Theta}}} p_{Z\boldsymbol{\Theta}}(z,\boldsymbol{\theta},t;\boldsymbol{x})\mathrm{d}\boldsymbol{\theta} = \sum_{q=1}^{n_{\mathrm{sel}}} \int_{\Omega_{\boldsymbol{\Theta}_q}} p_{Z\boldsymbol{\Theta}}(z,\boldsymbol{\theta},t;\boldsymbol{x})\mathrm{d}\boldsymbol{\theta} \approx \sum_{q=1}^{n_{\mathrm{sel}}} p_{Z\boldsymbol{\Theta}}(z,\boldsymbol{\theta}_q,t;\boldsymbol{x}), \tag{42}$$

or

$$p_W(w,\tau;\boldsymbol{x}) = \int_{\Omega_{\boldsymbol{\Theta}}} p_{W\boldsymbol{\Theta}}(w,\boldsymbol{\theta},\tau;\boldsymbol{x})\mathrm{d}\boldsymbol{\theta} = \sum_{q=1}^{n_{\mathrm{sel}}} \int_{\Omega_{\boldsymbol{\Theta}_q}} p_{W\boldsymbol{\Theta}}(w,\boldsymbol{\theta},\tau;\boldsymbol{x})\mathrm{d}\boldsymbol{\theta} \approx \sum_{q=1}^{n_{\mathrm{sel}}} p_{W\boldsymbol{\Theta}}(w,\boldsymbol{\theta}_q,\tau;\boldsymbol{x}). \tag{43}$$

9 References

Agrawal RK, Kaur B, Agarwal P (2021) Quantum inspired Particle Swarm Optimization with guided exploration for function optimization. Applied Soft Computing 102:107122. https://doi.org/10.1016/j.asoc.2021.107122

Aoues Y, Chateauneuf A (2010) Benchmark study of numerical methods for reliability-based design optimization. Structural and Multidisciplinary Optimization 41:277–294. https://doi.org/10.1007/s00158-009-0412-2

Au SK, Beck JL (2001) Estimation of small failure probabilities in high dimensions by subset simulation. Probabilistic Engineering Mechanics 16:263–277. https://doi.org/10.1016/S0266-8920(01)00019-4

Chen JQ, Tang YF, Ge R, et al (2013) Reliability design optimization of composite structures based on PSO together with FEA. Chinese Journal of Aeronautics 26:343–349. https://doi.org/10.1016/j.cja.2013.02.011

Chen JB, Li J (2009) A note on the principle of preservation of probability and probability density evolution equation. Probabilistic Engineering Mechanics 24:51–59. https://doi.org/10.1016/j.probengmech.2008.01.004

Chen JB, Li J (2005) Dynamic response and reliability analysis of non-linear stochastic structures. Probabilistic Engineering Mechanics 20:33–44. https://doi.org/10.1016/j.probengmech.2004.05.006

Chen JB, Li J (2007) The extreme value distribution and dynamic reliability analysis of nonlinear structures with uncertain parameters. Structural Safety 29:77–93. https://doi.org/10.1016/j.strusafe.2006.02.002

Chen JB, Yang JS, Jensen HA (2020) Structural optimization considering dynamic reliability constraints via probability density evolution method and change of probability measure. Structural and Multidisciplinary Optimization 62:2499–2516. https://doi.org/10.1007/s00158-020-02621-4

Chen JB, Yang JY, Li J (2016) A GF-discrepancy for point selection in stochastic seismic response analysis of structures with uncertain parameters. Structural Safety 59:20–31. https://doi.org/10.1016/j.strusafe.2015.11.001

Chen QD, Sun J, Palade V, et al (2022) An improved Gaussian distribution based quantum-behaved particle swarm optimization algorithm for engineering shape design problems. Engineering Optimization 54: 743-769. https://doi.org/10.1080/0305215x.2021.1900154

Cheng GD, Xu L, Jiang L (2006) A sequential approximate programming strategy for reliability-based structural optimization. Computers & Structures 84:1353–1367. https://doi.org/10.1016/j.compstruc.2006.03.006

Coelho L dos S (2010) Gaussian quantum-behaved particle swarm optimization approaches for constrained engineering design problems. Expert Systems with Applications 37:1676–1683. https://doi.org/10.1016/j.eswa.2009.06.044

Coleman JJ (1959) Reliability of aircraft structures in resisting chance failure. Operations Research 7:639–645. https://doi.org/10.1287/opre.7.5.639

Dimou CK, Koumousis VK (2009) Reliability-based optimal design of truss structures using particle swarm optimization. Journal of Computing in Civil Engineering 23:100–109. https://doi.org/10/10.1061/(ASCE)0887-3801(2009)23:2(100)

Du XP, Chen W (2004) Sequential optimization and reliability assessment method for efficient probabilistic design. Journal of Mechanical Design 126:225–233. https://doi.org/10.1115/1.1649968

Enevoldsen I, Sørensen JD (1994) Reliability-based optimization in structural engineering. Structural Safety 15:169–196. https://doi.org/10.1016/0167-4730(94)90039-6

Freitas D, Lopes LG, Morgado-Dias F (2020) Particle swarm optimisation: a historical review up to the current developments. Entropy 22:362. https://doi.org/10.3390/e22030362

Griffith DJ, Schroeter DF (2018) Introduction to quantum mechanics. Cambridge University Press, Cambridge.

Haftka RT, Adelman HM (1989) Recent developments in structural sensitivity analysis. Structural Optimization 1(3): 137-151.

Haftka RT, Gürdal Z (1992) Elements of structural optimization. Kluwer, Dordrecht.

Hamzehkolaei NS, Miri M, Rashki M (2016) An enhanced simulation-based design method coupled with meta-heuristic search algorithm for accurate reliability-based design optimization. Engineering with Computers 32:477–495. https://doi.org/10.1007/s00366-015-0427-9

Han KH, Kim JH (2000) Genetic quantum algorithm and its application to combinatorial optimization problem. In: Proceedings of the 2000 Congress on Evolutionary Computation, CEC00 (Cat. No.00TH8512) 2:1354–1360. https://doi.org/10.1109/cec.2000.870809

Jensen HA, Jerez D, Beer M (2021) A general two-phase Markov chain Monte Carlo approach for constrained design optimization: Application to stochastic structural optimization. Computer Methods in Applied Mechanics and Engineering 373:113487. https://doi.org/10.1016/j.cma.2020.113487

Jensen HA, Becerra LG, Valdebenito MA (2013) On the use of a class of interior point algorithms in stochastic structural optimization. Computers & Structures 126:69–85. https://doi.org/10.1016/j.compstruc.2013.01.008

Jensen HA, Jerez DJ, Valdebenito M (2020) An adaptive scheme for reliability-based global design optimization: A Markov chain Monte Carlo approach. Mechanical Systems and Signal Processing 143:106836. https://doi.org/10.1016/j.ymssp.2020.106836

Jerez DJ, Jensen HA, Beer M (2022) Reliability-based design optimization of structural systems under stochastic excitation: An overview. Mechanical Systems and Signal Processing 166:108397. https://doi.org/10.1016/j.ymssp.2021.108397

Jiang C, Qiu HB, Gao L, et al (2017) An adaptive hybrid single-loop method for reliability-based design optimization using iterative control strategy. Structural and Multidisciplinary Optimization 56:1271–1286. https://doi.org/10.1007/s00158-017-1719-z

Jiang ZM, Li J (2016) Analytical solutions of the generalized probability density evolution equation of three classes stochastic systems (in Chinese). Chinese Journal of Theoretical and Applied Mechanics 48:413–421. https://doi.org/10.6052/0459-1879-15-221

Kadowaki T, Nishimori H (1998) Quantum annealing in the transverse Ising model. Physical Review E 58:5355–5363. https://doi.org/10.1103/PhysRevE.58.5355

Kennedy J, Eberhart R (1995) Particle swarm optimization. In: Proceedings of ICNN'95 - International Conference on Neural Networks, IEEE 4:1942–1948. https://doi.org/10.1109/icnn.1995.488968

Li J, Chen JB (2009) Stochastic dynamics of structures. John Wiley & Sons (Asia) Pte Ltd, Singapore

Li J, Chen JB (2008) The principle of preservation of probability and the generalized density evolution equation. Structural Safety 30:65–77. https://doi.org/10.1016/j.strusafe.2006.08.001

Li J, Chen JB (2005) Dynamic response and reliability analysis of structures with uncertain parameters. International Journal for Numerical Methods in Engineering 62:289–315. https://doi.org/10.1002/nme.1204

Li J, Chen JB (2004) Probability density evolution method for dynamic response analysis of structures with uncertain parameters. Computational Mechanics 34:400–409. https://doi.org/10.1007/s00466-004-0583-8

Li J, Chen JB, Fan WL (2007a) The equivalent extreme-value event and evaluation of the structural system reliability. Structural Safety 29:112–131. https://doi.org/10.1016/j.strusafe.2006.03.002

Li J, Wang D (2023) Comparison of PDEM and MCS: accuracy and efficiency. Probabilistic Engineering Mechanics 71:103382. https://doi.org/10.1016/j.probengmech.2022.103382

Li LJ, Huang ZB, Liu F, et al (2007b) A heuristic particle swarm optimizer for optimization of pin connected structures. Computers & Structures 85:340–349. https://doi.org/10/d7pz6v

Li YY, Jiao LC, Shang RH, Stolkin R (2015) Dynamic-context cooperative quantum-behaved particle swarm optimization based on multilevel thresholding applied to medical image segmentation. Information Sciences 294:408–422. https://doi.org/10.1016/j.ins.2014.10.005

Liang JH, Mourelatos ZP, Nikolaidis E (2007) A single-loop approach for system reliability-based design optimization. Journal of Mechanical Design 129:1215–1224. https://doi.org/10.1115/DETC2006-99240

Liao KW, Biton NIDR (2019) A heuristic optimization considering probabilistic constraints via an equivalent single variable Pearson distribution system. Applied Soft Computing 78:670–684. https://doi.org/10.1016/j.asoc.2019.03.021

Liao KW, Biton NIDR (2020) A heuristic moment-based framework for optimization design under uncertainty. Engineering with Computers 36:1229–1242. https://doi.org/10.1007/s00366-019-00759-4

Liu TY, Jiao LC, Ma WP, et al (2016) Cultural quantum-behaved particle swarm optimization for environmental/economic dispatch. Applied Soft Computing 48:597–611. https://doi.org/10.1016/j.asoc.2016.04.021

Lutes LD, Sarkani S (2004) Random vibrations: analysis of structural and mechanical systems. Elsevier, Burlington.

Lyu MZ, Chen JB (2021) First-passage reliability of high-dimensional nonlinear systems under additive excitation by the ensemble-evolving-based generalized density evolution equation. Probabilistic Engineering Mechanics 63:103119. https://doi.org/10.1016/j.probengmech.2021.103119

Lyu MZ, Chen JB (2022) A unified formalism of the GE-GDEE for generic continuous responses and first-passage reliability analysis of multi-dimensional nonlinear systems subjected to non-white-noise excitations. Structural Safety 98:102233. https://doi.org/10.1016/j.strusafe.2022.102233

Ma F, Zhang H, Bockstedte A, et al (2004) Parameter analysis of the differential model of hysteresis. Journal of Applied Mechanics 71:342–349. https://doi.org/10.1115/1.1668082

Meng Z, Li G, Wang X, et al (2021) A comparative study of metaheuristic algorithms for reliability-based design optimization problems. Archives of Computational Methods in Engineering 28:1853-1869. https://doi.org/10.1007/s11831-020-09443-z

Nocedal J, Wright SJ (2006) Numerical optimization, 2nd ed. Springer, New York.

Petromichelakis I, Kougioumtzoglou IA (2020) Addressing the curse of dimensionality in stochastic dynamics: A Wiener path integral variational formulation with free boundaries. Proceedings of the Royal Society A 476:20200385. https://doi.org/10.1098/rspa.2020.0385

Psaros AF, Kougioumtzoglou IA (2020) Functional series expansions and quadratic approximations for enhancing the accuracy of the Wiener path integral technique. ASCE Journal of Engineering Mechanics 146(7):04020065. https://doi.org/10.1061/(ASCE)EM.1943-7889.0001793

Shi YH, Eberhart R (1998) A modified particle swarm optimizer. In: 1998 IEEE International Conference on Evolutionary Computation Proceedings, IEEE World Congress on Computational Intelligence (Cat. No.98TH8360) 69–73. https://doi.org/10.1109/ICEC.1998.699146

Shinozuka M (1972) Monte Carlo solution of structural dynamics. Computers & Structures 2:855–874. https://doi.org/10.1016/0045-7949(72)90043-0

Song W, Qiao YY, Park SC, et al (2015) A hybrid evolutionary computation approach with its application for optimizing text document clustering. Expert Systems with Applications 42:2517–2524. https://doi.org/10.1016/j.eswa.2014.11.003

Sun J (2009) Particle swarm optimization with particles having quantum behavior. Doctoral dissertation, Jiangnan University, China (in Chinese).

Sun J, Fang W, Wu XJ, et al (2012) Quantum-behaved particle swarm optimization: Analysis of individual particle behavior and parameter selection. Evolutionary Computation 20:349–393. https://doi.org/10.1162/evco_a_00049

Sun J, Feng B, Xu WB (2004a) Particle swarm optimization with particles having quantum behavior. In: Proceedings of the 2004 Congress on Evolutionary Computation 1:325–331. https://doi.org/10.1109/cec.2004.1330875

Sun J, Xu WB, Feng B (2004b) A global search strategy of quantum-behaved particle swarm optimization. In: IEEE Conference on Cybernetics and Intelligent Systems, 2004, 1:111–116. https://doi.org/10.1109/ICCIS.2004.1460396

Svanberg K (1987) The method of moving asymptotes—a new method for structural optimization. International Journal for Numerical Methods in Engineering 24:359–373. https://doi.org/10.1002/nme.1620240207

Svanberg K (2007) MMA and GCMMA-two methods for nonlinear optimization. In: Optimization and Systems Theory, KTH, Stockholm

Taflanidis AA, Beck JL (2008) Stochastic subset optimization for optimal reliability problems. Probabilistic Engineering Mechanics 23:324–338. https://doi.org/10.1016/j.probengmech.2007.12.011

Taflanidis AA, Beck JL (2009) Stochastic Subset Optimization for reliability optimization and sensitivity analysis in system design. Computers & Structures 87:318–331. https://doi.org/10.1016/j.compstruc.2008.12.015

Tu J, Choi KK, Park YH (1999) A new study on reliability-based design optimization. Journal of Mechanical Design 121:557–564. https://doi.org/10.1115/1.2829499

Valdebenito MA, Schuëller GI (2011) Efficient strategies for reliability-based optimization involving non-linear, dynamical structures. Computers & Structures 89:1797–1811. https://doi.org/10.1016/j.compstruc.2010.10.014

Valdebenito MA, Schuëller GI (2010) A survey on approaches for reliability-based optimization. Structural and Multidisciplinary Optimization 42:645–663. https://doi.org/10.1007/s00158-010-0518-6

Xi ML, Sun J, Liu L, et al (2016) Cancer feature selection and classification using a binary quantum-behaved particle swarm optimization and support vector machine. Computational and Mathematical Methods in Medicine 2016:e3572705. https://doi.org/10.1155/2016/3572705

Xue T, Li RF, Tokgo M, et al (2017) Trajectory planning for autonomous mobile robot using a hybrid improved QPSO algorithm. Soft Computing 21:2421–2437. https://doi.org/10.1007/s00500-015-1956-2

Yang IT, Hsieh YH (2011) Reliability-based design optimization with discrete design variables and non-smooth performance functions: AB-PSO algorithm. Automation in Construction 20:610–619. https://doi.org/10.1016/j.autcon.2010.12.003

Yang IT, Hsieh YH (2013) Reliability-based design optimization with cooperation between support vector machine and particle swarm optimization. Engineering with Computers 29:151–163. https://doi.org/10.1007/s00366-011-0251-9

Yang IT, Hsieh YH, Kuo CG (2016) Integrated multiobjective framework for reliability-based design optimization with discrete design variables. Automation in Construction 63:162–172. https://doi.org/10.1016/j.autcon.2015.12.010

Yang JS, Chen JB, Jensen HA (2022a) Structural design optimization under dynamic reliability constraints based on the probability density evolution method and highly-efficient sensitivity analysis. Probabilistic Engineering Mechanics 68:103205. https://doi.org/10.1016/j.probengmech.2022.103205

Yang JS, Jensen HA, Chen JB (2022b) Structural optimization under dynamic reliability constraints utilizing probability density evolution method and metamodels in augmented input space. Structural and Multidisciplinary Optimization 65:107. https://doi.org/10.1007/s00158-022-03188-y

Yang JS, Chen JB, Beer M, Jensen HA (2022c) An efficient approach for dynamic-reliability-based topology optimization of braced frame structures with probability density evolution method.

Advances in Engineering Software 173:103196. https://doi.org/10.1016/j.advengsoft.2022.103196

Yao F, Dong ZY, Meng K, et al (2012) Quantum-inspired particle swarm optimization for power system operations considering wind power uncertainty and carbon tax in Australia. IEEE Transactions on Industrial Informatics 8:880–888. https://doi.org/10.1109/tii.2012.2210431

Yu S, Wang ZL, Wang ZH (2019) Time-dependent reliability-based robust design optimization using evolutionary algorithm. ASCE-ASME Journal of Risk and Uncertainty in Engineering Systems Part B-Mechanical Engineering 5:020911. https://doi.org/10.1115/1.4042921

Zafar T, Zhang YW, Wang ZL (2020) An efficient Kriging based method for time-dependent reliability based robust design optimization via evolutionary algorithm. Computer Methods in Applied Mechanics and Engineering 372:113386. https://doi.org/10.1016/j.cma.2020.113386

Zhang X, Zhang JJ, Hu YT, et al (2020) Structural damage recognition based on the finite element method and quantum particle swarm optimization algorithm. IEEE Access 8:184785–184792. https://doi.org/10.1109/ACCESS.2020.3026068

Zhao YG, Lu ZH (2007) Fourth-moment standardization for structural reliability assessment. Journal of Structural Engineering 133:916–924. https://doi.org/10.1061/(ASCE)0733-9445(2007)133:7(916)

Zhao XG, Liang J, Meng J, et al (2020) An improved quantum particle swarm optimization algorithm for environmental economic dispatch. Expert Systems with Applications 152:113370. https://doi.org/10.1016/j.eswa.2020.113370

Zhong CT, Li G, Meng Z (2022) A hybrid teaching–learning slime mould algorithm for global optimization and reliability-based design optimization problems. Neural Computing and Applications 34:16617–16642. https://doi.org/10.1007/s00521-022-07277-3